Ecological Modelling 482 (2023) 110393

Contents lists available at ScienceDirect

Ecological Modelling

journal homepage: www.elsevier.com/locate/ecolmodel

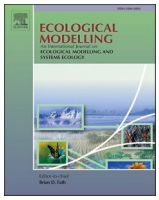

Simulating the migration dynamics of juvenile salmonids through rivers and estuaries using a hydrodynamically driven enhanced particle tracking model

Vamsi Krishna Sridharan, Ph.D. [a,*], Fisheries Collaborative Program University of California, Santa Cruz. Formerly affiliated with Southwest Fisheries Science Center, National Marine Fisheries Service, National Oceanic and Atmospheric Administration, Doug Jackson, Ph.D. [b], Andrew M. Hein, Ph.D. [c], Russell W. Perry, Ph.D. [d], Adam C. Pope [d], Noble Hendrix, Ph.D. [e], Eric M. Danner, Ph.D. [c], Steven T. Lindley, Ph.D. [c]

[a] Tetra Tech, 10306 Eaton Place, Fairfax, VA 22030, United States
[b] QEDA Consulting, LLC., 4007 Densmore Avenue N., Seattle, WA, 98103, United States
[c] Southwest Fisheries Science Center, National Marine Fisheries Service, National Oceanic and Atmospheric Administration, 110 McAllister Way, Santa Cruz, CA, 95060, United States
[d] U.S. Geological Survey Western Fisheries Research Center, Columbia River Research Laboratory, 5501A Cook-Underwood Road, Cook, WA 98605, United States
[e] QEDA Consulting, LLC., 5706 29th Avenue NE, Seattle, WA, 98105, United States

ARTICLE INFO

Keywords:
Agent-based model
Particle tracking model
Salmonid migration
Ecological model
Estuary
Hydrodynamics
Ecological management
Water resources management
Climate change

ABSTRACT

Juvenile salmonids migrate hundreds of kilometers from their natal streams to mature in the ocean. Throughout this migration, they respond to environmental cues such as local water velocities and other stimuli to direct and modulate their movements, often through heavily modified riverine and estuarine habitats. Management strategies in an uncertain future of climate change and altered land use regimes depend heavily on being able to reliably predict their ocean entry timings, route use, and survival rates through rivers and estuaries. We developed a spatially-explicit agent-based model of fish movement in response to hydrodynamic flows that uses movement dynamics gleaned from multi-dimensional tracking datasets of acoustically tagged juveniles moving through an urbanized, branched tidal estuary. We demonstrate how such models can be calibrated, and we apply it to the Sacramento-San Joaquin Delta in Central California. The quality of the out-of-sample validation of the model to predict juvenile salmon survival and route selection indicates that the model is versatile and flexible enough to be used in novel hydroclimatological conditions.

1. Introduction

The loss of estuarine habitat for iconic, endangered and economically important marine organisms is extensive around the world, leaving decision makers with the difficult task of ensuring reliable water supply for human uses while maintaining ecosystem services. While much is known about how rearing and migrating anadromous fish use estuarine habitats, at present we have limited ability to make quantitative predictions about how these fish are likely to respond to changes to their estuarine environment. Therefore, ecological models that provide sound understanding of the behaviors of aquatic species and contribute to realistic quantification of the population dynamics under altered hydroclimatologies are required for better understanding the resiliency of these species to changing landscapes, and for optimal water management.

In this paper, we describe the development of the Enhanced Particle Tracking Model (*ePTM*), a data- and theory-driven agent-based model of anadromous juvenile salmonid migration through rivers and estuaries using the outputs of a system-scale hydrodynamic flow model. In this model, we develop behavior agencies that are consistent across multiple scales of motion (tens of meters over a few minutes to hundreds of kilometers over several days), and can be inferred from observations. To demonstrate an application, we calibrate and validate this model for migrating juvenile Chinook salmon in the Sacramento-San Joaquin

* Corresponding author.
E-mail addresses: vasridha@ucsc.edu, vamsi.sridharan@tetratech.com (V.K. Sridharan).

https://doi.org/10.1016/j.ecolmodel.2023.110393
Received 21 July 2022; Received in revised form 15 April 2023; Accepted 20 April 2023
Available online 28 April 2023

Delta (hereafter, the Delta) in Central California.

Globally, salmonid species are widespread along temperate and subarctic coastlines and contributed nearly 15 billion dollars to the global fisheries in 2016 (Irarrazával and Bustos-Gallardo 2019). Many of the salmonid stocks are overexploited and a significant number of salmonid species are either threatened or critically endangered (Yeakley and Hughes 2014; Pauly 2018). Habitat stewardship is a common and significant component of freshwater and marine management plans for salmonids (Yeakley and Hughes 2014).

In the Delta, facilitating successful salmonid migrations is a water management goal that often conflicts with other demands on the system, such as extracting water from the estuary for agricultural or municipal use (Delta Stewardship Council 2019). Every year, four seasonal runs (Fall, Late Fall, Winter and Spring) of juvenile Chinook salmon (Johnson et al., 2017) and steelhead migrate to the Pacific Ocean through the Delta (MacFarlane and Norton 2002; Chapman et al., 2013), moving through diverse habitats, encountering predators, interacting with highly dynamic flows, and passing a multitude of human-made structures. Survival of juvenile salmonids migrating through the Delta can be extremely low (e.g., Perry et al., 2010; Perry et al., 2014; Michel et al., 2015; Perry et al., 2018; Buchanan and Skalski 2020). As a result, tools for predicting how water management actions will affect migrating salmonids are urgently needed (Delta Stewardship Council 2022).

Historically, juvenile salmonid migration rates and survival through rivers and estuaries have been estimated using statistical models (e.g., Newman 2003; Perry et al., 2018; Hance et al., 2020) or phenomenological models that represent net migration rates, overall dispersal and mortality through physically-inspired fate and transport models (e.g., Zabel and Anderson 1997; Zabel et al., 2008; Sridharan and Hein 2019). Statistical models only reliably describe patterns over the observed range of conditions, do not have emergent behaviors, and therefore have limited use in novel hydroclimatological and management conditions. At the other end of the spectrum are models that describe complex systems with dynamics that emerge due to the interactions of animal behavior in response to environmental stimuli. These include cognitive models of fish movement (e.g., Hein et al., 2018; Jhawar et al., 2020; Nadler et al., 2021) and fine-scale computational fluid dynamics and coupled biological random walk models (Goodwin et al., 2006; Gross et al., 2021) or simulated fish whose behavior is governed by machine learning (Arenas et al., 2015) or artificial intelligence (Olivetti et al., 2021). However, these models are too computationally intensive and are either too abstract (Hein et al., 2018; Jhawar et al., 2020; Nadler et al., 2021) or too domain-specific (Olivetti et al., 2021; Gross et al., 2021) to be useful as decision support tools.

Agent-based models with realistic behaviors driven by system-scale flow models, such as the *ePTM*, can help bridge the gap between simple models and highly refined models and have the potential to predict migration dynamics under novel conditions. Agent-based models have been developed for fish movement and migration in the past (e.g., Massoudieh et al., 2011; Bracis and Anderson 2012; Kimmerer and Rose 2018; Gross et al., 2020; Morrice et al., 2020; Lai 2022), but have typically involved simple or ad-hoc animal behaviors. The behavioral complexity represented in the *ePTM* is based on tagged salmonid migration data and theoretical expectations from the literature. These behaviors allow us to capture the shifts in behavior of salmonids as they migrate through complex estuaries and to physically represent real-world systems. These features are likely limited in simpler models, or are abstracted from intuitive understanding in artificial intelligence-based models, and in the case of ad-hoc agent-based models, cannot be explained directly using the available data.

We organize the paper as follows: In Section 2, we provide a brief background of the migration dynamics of juvenile anadromous salmonids. In Section 3, we use the insights gained from Section 2 to describe the structure of the *ePTM*. In Sections 4 and 5, we calibrate and validate the model for a specific system, and evaluating the sensitivity of the migration statistics to the model parameters. In Section 6, we present ways in which the model can be used as a numerical laboratory as well as a decision support tool for water management.

2. Juvenile salmonid migration and survival dynamics

In order to build our migration model, we (i) reviewed the literature on anadromous juvenile salmonid migration to identify common patterns in animal movement, (ii) engaged with local and regional stakeholders in Central California to incorporate anecdotal evidence about the natural history of salmonids, and (iii) performed our own analyses of datasets obtained in the Delta from acoustic telemetry arrays which provided system-wide coverage in the form of detection histories of fish at various points along the river system (Perry et al., 2010; San Joaquin River Group Authority 2013; Perry et al., 2018; Notch et al., 2020), and high-resolution planar two-dimensional fish tracks [AECOM et al. 2015; California Department of Water Resources (DWR) 2015; R.W. DWR 2016] from two locations to quantify the key aspects of migration behavior directly from data (Raimondi et al., 2021). Using these datasets, we identified five key behavioral elements of salmonid migration: (i) active swimming, (ii) orientation towards or away from the ocean, (iii) holding relative to the flow, (iv) routing at channel junctions, and (v) mortality due to predation. We subsequently discuss these elements as they apply to model design.

2.1. Active swimming behavior

While larval life-stages of some fish species passively drift with the flow (Nagel et al., 2021), migrating juvenile salmonids actively propel themselves relative to the flow. To describe fish movement in this paper, we define *swimming velocity* (directed) or *speed* (undirected) as the movement rate of the fish relative to the water over a short timescale (a few minutes), the *overground movement velocity* as the directed combined movement rate of the fish and the water over a short timescale, and the *migration rate* as the displacement per unit time of the fish through the river system over a long timescale (several days). Several studies have shown some common patterns in salmonid migration: (i) movement away from their natal streams (e.g., Sturrock et al., 2015), (ii) swimming velocities within individual fish that vary over time (e.g., Lehman et al., 2017), and (iii) in regions of estuaries where the tidal flow reverses, migration rates that are faster when flow oceanward is faster, and slower when flow oceanward is slower (McCormick et al., 1998). These results indicate that salmonid swimming speeds vary both spatially and temporally throughout the system, and among individuals.

2.2. Orientation toward or away from the ocean

Orientation relative to the flow in tidal estuaries has received much attention in the acoustic tagging literature. Numerous studies have found that until they encounter a salinity threshold close to the point of ocean entry, fish swim actively with the direction of flow during the ebb or oceanward flow phase of the tide, and do not effectively move during the flood or landward flow phase of the tide (McCleave 1978; Solomon 1978; Healey 1980; McCormick et al., 1998; Moore et al., 1998; Hedger et al., 2008). In the lower estuary close to the ocean downstream of this salinity threshold, fish mostly swim towards the ocean (Lacroix and McCurdy 1996; McCormick et al., 1998; Moore et al., 1998; Hedger et al., 2008). In tidally reversing regions, Kelly and Klimley (2012) reported that non-salmonid anadromous fish orient somewhat randomly during slackwater, or periods of low flows between tidal reversals. Acoustic telemetry studies in tidal parts of the Delta have also reported positive rheotaxis, or orientations against the flow in regions with strongly unidirectional oceanward flow, as well as fish tracks exhibiting back-and-forth lateral movements across the river during low freshwater flows (DWR 2015; R.W. DWR 2016). These results indicate a potential shift in the behavior of salmonids in response to the transition from unidirectional river flows to bidirectional flows in the estuary.

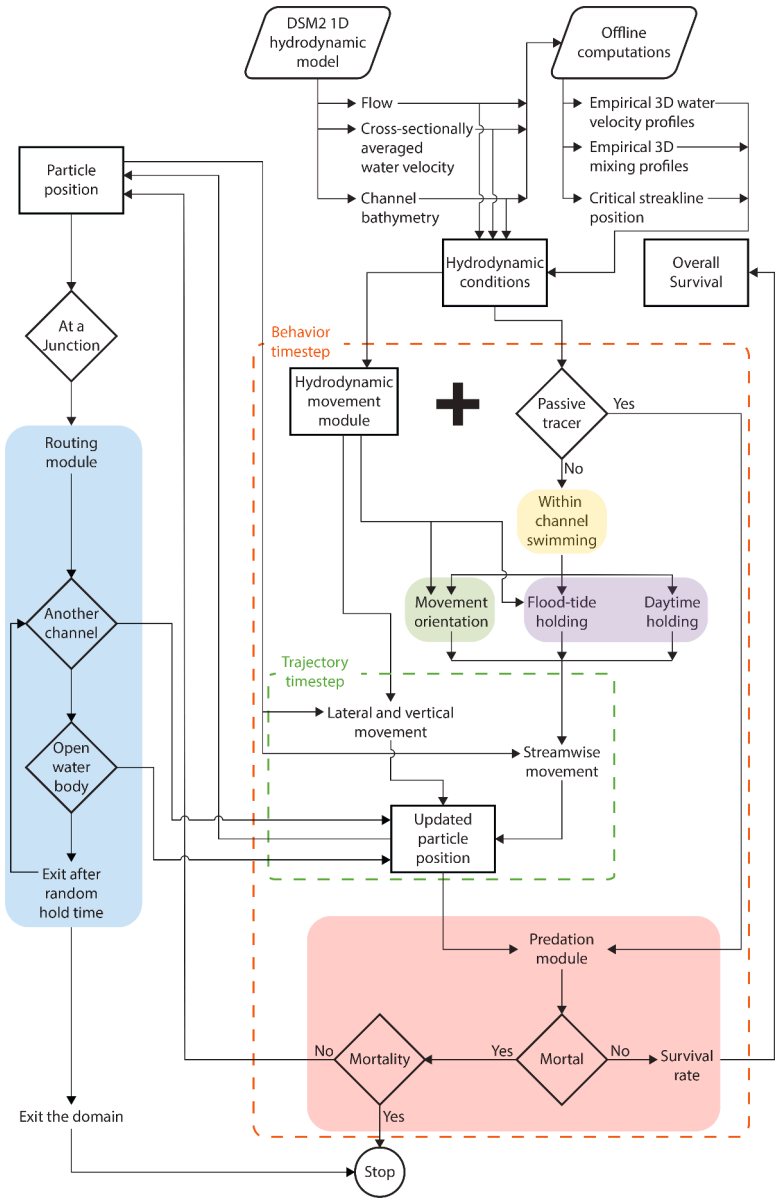

Fig. 1. Model structure. Model inputs, outputs and decision points are shown respectively as parallelograms, rectangles and rhombuses. The five key biological processes are highlighted. The dashed boxes indicate the biological timestep and trajectory sub-timestep respectively. The key processes occur over each timestep to update a simulated particle's position. Model computations stop when a particle either dies or exits the system.

2.3. *Holding relative to the flow*

In this paper, we define *holding* as a behavior that results in no net displacement over some short period (over a few minutes). Authors have reported two types of holding behaviors: (i) holding related to flow, and (ii) holding related to the day/night cycle. In general, holding is likely governed by proximity to the ocean. In regions where the tidal flow reverses, fish have been observed to hold against the flow or move slowly oceanward during the landward phase of the flow (Lacroix and McCurdy 1996; Miller and Sadro 2003; Lacroix et al., 2005). Some studies have reported a statistically significant preference among juvenile salmonids to migrate oceanward at night in regions of the river system where the flow is non-reversing, and a more photo-period-agnostic migration pattern throughout the whole day as fish move closer to the ocean (Moser et al., 1991; Lacroix and McCurdy 1996; Hedger et al., 2008; Chapman et al., 2013).

Some of these behaviors were also corroborated by observations by domain experts (National Marine Fisheries Service 2021). In particular, selective holding of fish during the landward phase of the tide (Forward and Tankersley 2001; Verhelst et al., 2018), preferential nighttime migration in the non-reversing tidal regions of the Delta, and more uniform migration patterns throughout the day in the tidal parts of the system were observed by domain experts.

2.4. *Routing at river junctions*

In general, migratory fish do not move through channel junctions in river networks or branched tidal estuaries as neutrally buoyant suspended material (Steel et al., 2013; Ramón et al. 2018). Recently, two models have represented route selection processes significantly better than models which allow fish to randomly select a migration route. The critical streakline [Perry et al., 2014, R.W. 2016 (see their Box 3 for a summary); Hance et al., 2020] and the bifurcating streamline (Sridharan et al., 2018a) models both allow fish to enter a channel depending on its position relative to the streamline that bifurcates the flow into downstream channels at a river junction.

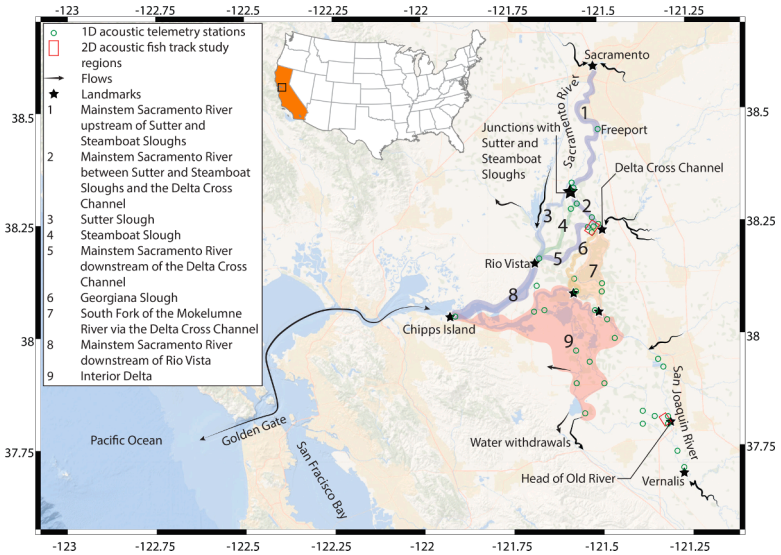

Fig. 2. Map of the San Francisco Bay-Delta system with regions over which the *ePTM* is calibrated. The inset map geolocates the Bay-Delta (box) within California (shaded orange) in the United States.

2.5. Mortality due to predation

Past analyses suggest that mortality due to predation is important in estuaries such as the Delta, resulting in relatively low survival (Perry et al., 2018; Pope et al., 2021) that is spatially variable (Perry et al., 2018; Hance et al., 2020; Michel et al., 2020; C.J. Michel et al. 2021; Notch et al., 2020). Anderson et al. (2005) proposed a mean-field theory of predation-driven mortality, the *XT* model, in which survival is a function of local predator density, the distance traveled by migrants through the predator field, *X*, the exposure time of migrants to predators, *T*, and the random velocities of predators and prey. This model has been shown to be consistent with survival patterns of Chinook salmon migrating through the Snake and Columbia Rivers (Anderson et al., 2005), and in the Sacramento River (Steel et al., 2020).

3. Model structure

The *ePTM*, written in modular object-oriented style in Java, is a three-dimensional coupled physical-biological Lagrangian particle tracking model that simulates the movements and mortality of juvenile salmonids through a river or estuary (Sridharan et al., 2021). The advantage of agent-based models such as the *ePTM* is the relative ease of specifying and modifying different behaviors one might wish simulated fish to follow. In the *ePTM*, the behaviors of simulated fish combine additively with the local water velocity (see also Olivetti et al., 2021), a feature that makes it easy to modify assumptions about physical forcing, the processes that determine locomotion, or both. Formally, this decomposition allows us to write the overground movement velocity of a given individual within a simulation timestep as

$$u = u_S + u_H \tag{1}$$

where $u > 0$ is oceanward movement and $u < 0$ is landward movement, u_S is an individual's swimming velocity, and u_H is the hydrodynamic velocity of the water in the individual's vicinity.

There are four major assumptions in the *ePTM*: (i) very small-scale auto-correlated sensory responses at sub-second timescales are assumed to be represented by stochastic noise (Codling et al., 2008), (ii) there is only a one-way coupling between the flow and fish movement, i.e., fluid-structure interactions through which fish may alter the flow field are not modeled, (iii) all simulated individuals follow the same stochastic behavioral rules, and (iv) interactions among individuals are weak enough that a reasonable approximation of migration behavior can be achieved by simulating many non-interacting individuals (but see Berdahl et al., 2016). For timescales on the order of 15 min (the typical timestep size at which movement is represented in the *ePTM*), the modifications of the flow field by the fish will average out so that fluid-structure interactions (e.g., Filella et al., 2018) can be safely ignored. Sridharan and Hein (2019) showed that the application of a one-dimensional advection-dispersion model that is based on these assumptions is able to recover the distribution of travel times of migrating steelhead in the Delta.

The structure of the *ePTM* is designed around five behavior modules to simulate the key processes related to juvenile salmonid migration discussed in Section 2 (Fig. 1). At each simulation timestep, simulated fish move through the water body where they are located, experience a probability of mortality due to predation, and, if they are in the vicinity of a river junction, move into one downstream water body or the other. By iterating this process over many timesteps, the *ePTM* produces predictions about how populations of migrants move, and when and where mortality occurs.

3.1. Model domain

In order to explore the structure of a model as complex as the *ePTM*, we ground-truthed it in the Sacramento-San Joaquin Delta (Fig. 2). The Delta is an estuary that has been highly modified by diking, channelization, water extraction, invasive species, and land reclamation, and is vulnerable to climate change, land subsidence, sea-level rise and salinity intrusion. Mortality of migrants is very high in the Delta, likely due to increased predation in highly channelized habitats with invasive aquatic plants (Moyle et al., 2010; Michel et al., 2020), alterations of natural flows by water operations (Kimmerer 2008), and favorable thermal tolerance regimes of native and invasive predators (C.J. Michel et al. 2021). However, recent studies have shown that there is a positive relationship between freshwater inflow and survival of migrating salmonids in the Delta (Perry et al., 2018; Buchanan and Skalski 2020; Hance et al., 2020; Michel et al., 2015; C.J. 2021), indicating that the high mortality might likely be alleviated by favorable flow conditions.

The Delta is an inverted alluvial fan estuary at the confluence of the Sacramento and San Joaquin Rivers, with its oceanward end at San Francisco Bay. Both the Sacramento and San Joaquin Rivers are rain- and snow-fed and heavily regulated by dams, with flows typically ranging from 200 to 2000 m^3/s in the Sacramento River and about 10 to 20% of that in the San Joaquin River. California State and Federal

Table 1
Calibration parameters in the *ePTM*.

Behavior element	Description	Parameter	Prior bounds	Units
Active swimming	Mean swimming speed	$\|\bar{u_S}\|$	$[0, 0.5]$	m/s
	Standard deviation of swimming speed	$\sigma_{\|u_S\|}$	$[0, 0.5]$	m/s
Orientation	Probability of memory persistence	p_M	$[0, 1]$	–
	Complement of the probability of rheotaxis	$\widetilde{P}_{\text{Rheotaxis}}$	$[0, 1]$	–
	Half-saturation point of logistic function	c	$[-10, 10]$	–
	Slope of logistic function	b	$[0, 10]$	–
Holding	Landward holding threshold water velocity	u_F	$[0, 1.5]$	m/s
	Holding probability above threshold	p_H	$[0, 1]$	–
	Daytime swimming probability	p_{DS}	$[0, 1]$	–
Mortality	Length-scale of survival decay	λ	$[10, 1000]$	m
	Time-dependence parameter	ω	$[0, 2]$	m/s

pumping facilities in the South Delta withdraw 10 to 50% of the inflow of freshwater from the system (Fig. 2) by operating sluice gates in the North Delta at the Delta Cross Channel which feed pumps that supply a network of canals moving water south (Fig. 2). Sridharan et al. (2018b) discuss the hydrodynamics of this system in detail.

3.2. Hydrodynamics and physical forcing on simulated fish

We based the *ePTM* on the California Department of Water Resources' (DWR) Delta Simulation Model II (*DSM2*) particle tracking module (DWR 1998). *DSM2* is a one-dimensional subgrid shallow water equation solver that provides the mean along-stream water velocities at grid points spaced roughly 1–5Km apart, and is used to drive the behaviors in the *ePTM*. In the *ePTM*, we disaggregate these mean velocities for both straight and curved channels (the lateral and vertical water velocity structures are parametrized as described in Appendix A) [DWR 1998]. The *ePTM* uses numerical methods that ensure consistency with the underlying model assumptions (Sridharan et al., 2018a) and, most importantly, it incorporates data- and theory-driven models of juvenile salmonid behavior during migration.

Although the positional variable of primary interest is the along-stream location of each individual, $x(t)$, we also track the location of each individual at each time in the lateral, $y(t)$, and vertical, $z(t)$, dimensions. $y(t)$ is specified as positive from the channel centerline to the right bank looking downstream, and $z(t)$ is specified as positive from the channel bottom to the free surface. Over a small time, Δt, positions are updated according to the following equations (Visser 1997):

$$\begin{aligned} x(t+1) &= x(t) + [u_H + u_S]\Delta t \\ y(t+1) &= y(t) + R_y\sqrt{2\varepsilon_H \Delta t} + \frac{d\varepsilon_H}{dy}\Delta t \\ z(t+1) &= z(t) + R_z\sqrt{2\varepsilon_V \Delta t} + \frac{d\varepsilon_V}{dz}\Delta t \end{aligned} \tag{2}$$

Here, u_H, u_S, and the vertical gradient of the vertical eddy diffusivity, $\frac{d\varepsilon_V}{dz}$, are all evaluated at the point $\{x(t), y(t), z(t), t\}$, while the spatially variable vertical eddy diffusivity is evaluated at the point $\left\{x(t), y(t), z(t) + \frac{1}{2}\frac{d\varepsilon_V}{dz}\Delta t, t\right\}$. ε_H, the spatially variable horizontal eddy diffusivity, is evaluated at the point $\left\{x(t), y(t) + \frac{1}{2}\frac{d\varepsilon_H}{dy}\Delta t, z(t), t\right\}$. R_y and R_z are uniformly distributed random numbers between –1 and 1. In the *ePTM*, we have included channel curvature, water velocity and turbulent mixing profiles with at least as much realism as a one-dimensional hydrodynamic model with a zeroth order turbulence closure will allow (Section A.1 in Appendix A). In order to represent particle trajectories realistically and balance the requirements of fidelity and performance, we tuned several model settings (see Appendix A). The profiles of u_H, ε_H and ε_V are obtained under the parametrizations in Appendix A.

The rationale behind the formulation in the system of Equations (2) is that simulated fish are pushed laterally and vertically due to random turbulent fluctuations. In reality, fish also move actively laterally and vertically within the water column in ways that likely depend on the morphologies of specific areas within the domain (Olivetti et al., 2021; Gross et al., 2021). The net effect of the system of Equations (2) is that behavior is adopted in the streamwise direction, and passive particle-like movements are applied in the lateral and vertical directions. This compromise retains the generality of the model.

3.3. Simulation timescales

The *ePTM* model simulates processes with two distinct timesteps. The primary timestep (τ) is 15 min and the sub-timestep (Δt) is 20 s. At every timestep, the behavioral decisions of each individual are updated and mortality is evaluated, while at every sub-timestep, the positions of each individual are updated (see section A.2 in Appendix A). This finer time resolution helps resolve uncorrelated movements relative to flows and total path length during a 15-minute interval. We chose the 15-minute timestep to ensure scalability in multi-decadal water management scenario evaluations, in which millions of fish have to be simulated over long durations. Given the 15-minute timestep, simulated fish behaviors in the *ePTM* should be interpreted as temporally-coarsened representations of cognitive responses to instantaneous local stimuli exhibited by migrants, which vary on spatial scales of a few meters and temporal scales of a few seconds (Olivetti et al., 2021). However, variability among individual migrants is maintained in the model.

The outcome of behavioral decisions at each timestep is stochastic, and they are produced by a set of behavioral functions that result in actions based on the location of the animal within the system and the environmental conditions at that location. We selected the forms of these functions on the basis of a review of the literature on migrating salmonids, as well as empirical evidence from our analyses of salmonid migration behavior in the Delta (Section 2). These functions also represent a tradeoff with the simplifying assumptions that is necessary to ensure that parameters are statistically identifiable and that computation times are tractable.

3.4. Active swimming behavior

Active swimming in the *ePTM* involves only along-stream movements induced by fish behavior. Locomotion in *ePTM* involves a sequence of behavioral choices each individual makes at each timestep. We represent these behaviors as a hierarchy of stochastic decisions to (i) first either hold position relative to the flow or swim, and (ii) subsequently, if they decide to swim, then to select the swimming direction and the swimming speed.

The swimming speeds of migratory salmonids vary over time, across environmental conditions, and in different regions of an estuary (Olivetti et al., 2021). To allow swimming speed to vary from one timestep to another and among individuals, we draw a random swimming speed for each individual that is not holding at each point in time. The swimming speed, $|u_S|$, for each individual at each timestep is drawn from a log-normal distribution of the form

$$\ln\mathrm{N}(\mu, \sigma) \sim \frac{1}{|u_S|\sigma\sqrt{2\pi}} e^{-\left[\frac{(\ln|u_S| - \mu)^2}{2\sigma^2}\right]} \tag{3}$$

where the parameters are given by

$$\mu = 2\ln|\bar{u_S}| - \frac{1}{2}\ln\left(\sigma^2_{|u_S|} + |\bar{u_S}|^2\right)\sigma = \sqrt{\ln\left(\sigma^2_{|u_S|} + |\bar{u_S}|^2\right)} - 2\ln|\bar{u_S}| \quad (4)$$

in which the mean swimming speed and standard deviation in observed swimming speeds are respectively $|\bar{u_S}|$ and $\sigma^2_{|u_S|}$ (Table 1). As salmonid swimming behavior could change over the course of migration with proximity to the ocean, we allow the parameters of the log-normal distribution to vary among different regions of the estuary as the simulated fish move through the system. To ensure that randomly drawn swimming speeds remain within the range of biologically plausible speeds, the log-normal distribution is truncated at the 95th percentile and rescaled appropriately.

3.5. Orientation towards or away from the ocean

The direction of along-stream swimming relative to flow varies across the system and over environmental conditions (Olivetti et al., 2021). To allow this in the *ePTM*, we incorporate a probabilistic swimming direction rule that determines each individual's swimming direction at each timestep. The swimming direction is influenced by the individual's previous swimming direction, as well as the flow it experiences. The structure of this rule is based on empirical patterns in the high-resolution fish tracks (AECOM et al. 2015; DWR 2015; R.W. 2016). While migrants regularly turn to direct locomotion landward, oceanward, or toward channel banks, they also exhibit a tendency to persist in a given swimming direction for long periods of time (Olivetti et al., 2021). To capture this tendency to persist, an individual is allowed to continue moving along its previous swimming direction (either oceanward or landward) at each simulation timestep with probability p_M (Table 1). The decision to persist is then determined by a Bernoulli trial with probability p_M.

If the Bernoulli draw to determine persistence results in a zero, the individual's swimming direction is determined by a stochastic decision based on the flow it experiences during the current timestep. This is motivated by the observation that fish in different flow regimes exhibit different tendencies to swim with or against prevailing flow (Olivetti et al., 2021). A range of processes have been attributed to flow detection by fish (Liao 2007; Burke et al., 2014; Klimley et al., 2017; Oteiza et al., 2017; Lohmann and Lohmann 2019; Miles et al., 2021). Regardless of the sensory mechanisms, strong flows are significantly easier to perceive compared to very weak flows. A simple way to represent this flow-strength-based perception is to model the probability of orienting in the direction of prevailing flow as a function of the dimensionless water velocity magnitude,

$$\tilde{u} = |u_H|/|\bar{u_H}| \quad (5)$$

where $|u_H|$ is the instantaneous water velocity magnitude at the migrant's location and $|\bar{u_H}|$ is the historical average water velocity in the system. The quantity $|\bar{u_H}|$ serves simply to normalize $\tilde{u}$ to a consistent range of values and any other constant could be used in its place without loss of generality (i.e., we are not assuming that fish have knowledge of the historical average water velocity). We assume water velocity magnitude is related to the individual's probability of orienting in the direction of the prevailing flow according to the function:

$$p_{\mathrm{SWF}}(t) = 0.5 + (\widetilde{P}_{\mathrm{Rheotaxis}} - 0.5)\left[\frac{1}{1 + e^{-(c+b\log\tilde{u})}}\right] \quad (6)$$

where p_{SWF} is the probability of orienting in the direction of flow, $\widetilde{P}_{\mathrm{Rheotaxis}}$ (read as the complement of the probability of rheotaxis) is a calibration parameter determined by where the migrant is located in the system, c is half-saturation point (the abscissa of the inflection point) and b is the slope of the steepest part of the curve (Table 1). If an individual is not holding, and not persisting in its previous movement direction, its direction relative to the flow is determined by a Bernoulli draw with probability given by $p_{\mathrm{SWF}}(t)$ from Eq. (6).

For positive values of c and small values of b, simulated fish exhibit sluggish responses to flow signals, i.e., an individual will make decisions that are not random only at very strong water speeds. For negative values of c and large values of b, simulated fish exhibit very sharp responses to small changes in the flow, i.e., decisions will be nonrandom even for weak flows. The $\widetilde{P}_{\mathrm{Rheotaxis}}$ parameter determines if the individual is likely to orient with or against the flow. If $\widetilde{P}_{\mathrm{Rheotaxis}} \approx 0$, then as flows become stronger, individuals will have a tendency to orient against the flow, or perform positive rheotaxis. If $\widetilde{P}_{\mathrm{Rheotaxis}} \approx 0.5$, orientation decisions will be random. If $\widetilde{P}_{\mathrm{Rheotaxis}} \approx 1$, then as flows become stronger, individuals will have a tendency to orient with the flow, or perform negative rheotaxis. By allowing these parameters to vary in different regions of the system, spatial variation in responses to flows can be captured.

3.6. Holding relative to the flow

In the *ePTM*, whether an individual will hold or swim during a given simulation timestep is determined by two factors: the time of day, and the phase of the tide. These dependencies are implemented by the following equations

$$P(\mathrm{Hold}) = \begin{cases} p_H; u_H < u_F \\ \mathbf{I}_{t\in\{D\}}(1 - p_{DS}); u_H \geq u_F \end{cases} \quad (7)$$

where, $p_H$is a probability that the individual holds, u_F is a landward flow threshold above which simulated fish are assumed to hold, $\mathbf{I}_{t\in\{D\}}$ is an indicator function denoting whether it is day (1) or night (0), and p_{DS} is the probability of swimming during the daytime (Chapman et al., 2013; Table 1). A migrant's decision to hold is determined by a Bernoulli trial with probability $P(\mathrm{Hold})$ at each timestep. This allows the model to capture different types of holding behavior observed in the system.

3.7. Routing at river junctions

In the *ePTM*, we allow simulated fish to move into downstream water bodies at junctions depending on their lateral position relative to the critical streakline or bifurcating streamline (Appendix A). When a migrant reaches the end of a river channel within a sub-timestep, the routing process is invoked, and it is moved into a downstream river or open water body (such as a flooded island or shallow lake). Subsequently, the remaining trajectory computation is completed for that sub-timestep in the new channel beginning from a random cross-sectional position. If an individual enters an open water body, it waits for a random length of time smaller than one day and then leaves the open water body randomly into a connecting downstream water body. While it would be straightforward to implement stochastic routing decisions that depend on the flow, the individual's lateral position, and other system- and species-specific attributes (see Steel et al., 2013; Hance et al., 2020), but we have not implemented this in the *ePTM* as we wanted to retain generality across species and flow conditions.

Recently, nonphysical barriers and fish guidance mechanisms such as bubble curtains and strobe lights have been investigated to steer fish into favorable migration routes in the Delta (Perry et al., 2014; DWR 2015; R.W. DWR 2016). These mechanisms work by directing fish away from a potentially deleterious route without altering the flow, and operate with some efficiency, η. We implement such mechanisms in the model as a "synthetic barrier," which restricts simulated fish from entering a specific water body during some fraction, η, of the time. Any number of barriers can be applied at any junction in the system domain with specified efficiencies. Over the duration of a simulation, such barriers will simply divert a fraction of simulated fish, η, into the next nearest downstream water body that does not have a barrier. While not fully realistic, the barrier mechanism nevertheless allows us to capture

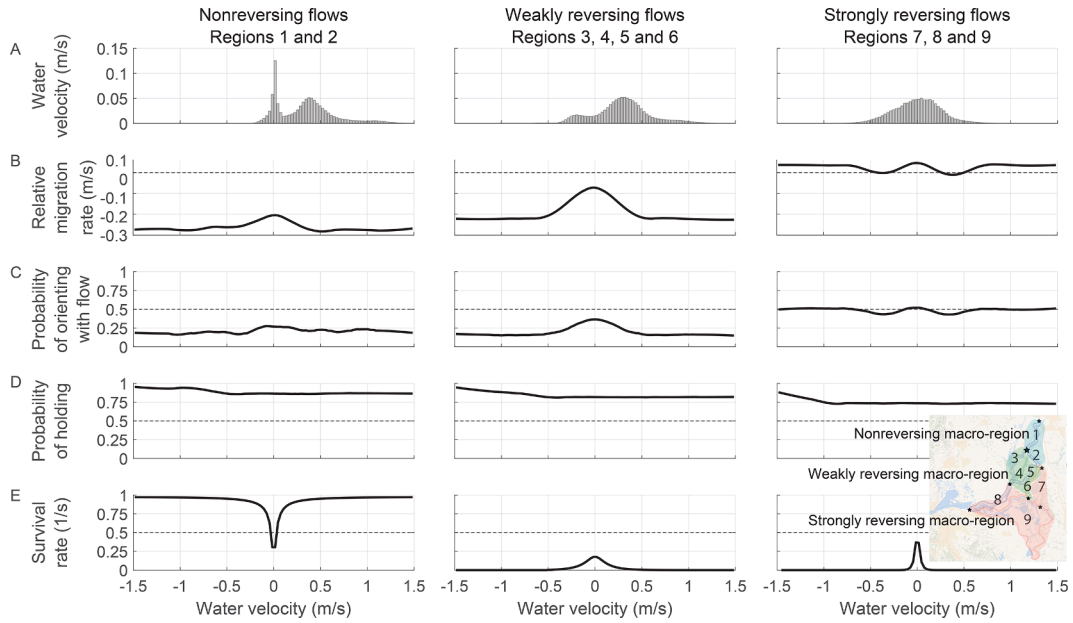

Fig. 3. Functional responses of behavior modules in the *ePTM* calibrated for salmonid migration in the Sacramento-San Joaquin Delta in the three macro-regions delineated in the inset map (the nine calibration regions are also shown as polygons): A. Histograms of instantaneous water velocities in the Sacramento-San Joaquin Delta and, as a function of the local environmental conditions (water velocity) experienced by a simulated fish, B. mean migration rate relative to flow, C. the probability of orienting with flow over a period of five days, D. the probability of holding over a period of five days, and E. the survival rate due to predation mortality. See Appendix B for details on how these quantities are estimated. In B, the dashed lines indicate that the migration rate relative to flow is negligible. In C, D and E, the dashed lines indicate random chance.

the leading order function of such barriers (see Section 5.3 below).

3.8. Predation and mortality

Survival in the *ePTM* is modeled using a modified version of the *XT* model developed in Anderson et al. (2005). The modification arises because we compute survival over the actual path of an individual in our model rather than over a fixed distance (see Appendix A). This modification follows from tracking simulated fish trajectories in the *ePTM*.

The basic assumption of the *XT* model is that, on average, the risk that prey migrating through a field of resident predators will be eaten by predators within a region can be expressed as constant per-unit distance and per-unit time rates. Our model computes survival probability of each individual in each 15-minute timestep as a function of two quantities: the total distance traveled by that individual in the timestep, X, and the duration of the timestep as:

$$P(\text{Survival}) = e^{-\frac{\sqrt{X^2+\omega^2\tau^2}}{\lambda}} \tag{8}$$

In the model, $t = \tau$. Here, the free parameters λ and ω respectively quantify how survival decays with distance traveled through a region, and represent stochasticity in the predator-prey encounters (Table 1). The difference between λ in Eq. (8) and in the Anderson et al. (2005) formulation is that in the former case, this parameter has to be inflated as a consequence of using the distance over migrant trajectories instead of river reach lengths (Appendix A). The difference in ω in the *ePTM* is that this parameter also captures the stochasticity in flow and fish trajectories (Appendix A). Thus, the parameter values in Eq. (8) will generally be much larger than in the conventional formulation of the *XT* model.

Typically, smaller values of λ represent denser predator fields, while larger values represent sparse predator distributions. Small values of ω represent a smaller contribution of the random (undirected) components of predator and prey movements to the overall encounter rates. Conceptually, small values of ω may be thought of as representative of stationary predators, whereas large values as representative of roving predators. In the *ePTM*, as we allow these parameters to spatially vary, the home ranges of different types of predators can be potentially represented in the model.

In standard applications, if a random draw from a uniform distribution is smaller than the probability of survival, an individual continues to move through the system. Otherwise, it is killed and the simulation terminates for that individual. An alternate mode is also available in the model wherein particles are not removed from the computation but rather continue to be simulated. Survival estimates can then be provided for each region, and compounded over the course of migration, using a fixed population of simulated migrants.

3.9. ePTM behavior kinetics

The functional responses of the behavior modules described in Sections 3.4 to 3.6 and 3.8 to local environmental conditions observed by simulated fish (i.e., instantaneous water velocities) calibrated for salmonids migrating through the Delta indicate the biological realism in the model. These responses are sketched in Fig. 3 (see Appendix B for details on how the responses were sketched). The parameter estimation process and optimal parameter values are reported below in Sections 4 and 5. To simplify the subsequent discussion, we grouped areas in the Delta into three macro-regions based on the flow characteristics modeled using *DSM2*. These are the nonreversing flow, weakly reversing flow and strongly reversing flow macro-regions, which each have distinctive instantaneous water velocity histograms (Fig. 3A). In all subsequent rows of Fig. 3, we aggregated behavior responses within all regions constituting each macro-region. Mean migration rate relative to the flow, orientation, holding and mortality dynamics are illustrated in Figs. 3B, C, D and E by assuming that simulated fish experience constant water velocities in each bin of the histograms shown in Fig. 3A over a period of five days.

By applying the swimming speed distribution in Eq. (2) and by using the orientation and holding probabilities from Eqs. (6) and (7), we obtain the mean relative migration rate as a function of water velocity in Fig. 3B (see Appendix B). From nonreversing to reversing macro-regions, the mean relative migration rate generally increases monotonically from

Table 2
Details of the late fall-run Chinook calibration dataset.

S. No.	Period	Mean flow during Delta entry (m^3/s)	Number of fish Released	Mean forklength of fish (mm)
1	5–6 Dec. 2006	496.1	65	166
2	17–18 Jan. 2007	492.0	81	163.9
3	4–7 Dec. 2007	442.4	209	152.9
4	15–18 Jan. 2008	750.2	212	154.7
5	30 Nov.–6 Dec. 2008	318.2	293	149.5
6	13–19 Jan. 2009	358.6	293	153.7
7	2–5 Dec. 2009	476.5	233	154.0
8	16–19 Dec. 2009	584.1	205	155.1

slower to slightly faster than the water velocity.

The probability of orienting with the flow estimated using Eq. (6) is typically much lower than random in the nonreversing and weakly reversing macro-regions, except during slack-water, indicating a tendency for positive rheotaxis in these regions. In the strongly reversing macro-region, this probability is close to random (Fig. 3C; see Appendix B).

Very rarely do water velocities ever exceed the flood phase holding threshold under historic conditions. The combined probability of holding due to strong flood phase landward flows and daylight estimated using Eq. (7), is typically about 0.75 without an appreciable trend through the domain (Fig. 3D; see Appendix B).

Mortality due to predation, estimated using Eq. (8) and by assuming that simulated fish (i) drift passively towards the ocean with the unidirectional freshwater current in the nonreversing macro-region and (ii) experience tidal excursions and a net oceanward Stokes' drift (Smythe 2020) in the reversing macro-regions, is typically low in the nonreversing macro-region and significantly increases in the tidally reversing macro-regions (Fig. 3E; see Appendix B). This is due to the increased path lengths and travel times in the reversing macro-regions. Survival in the nonreversing macro-region dips near slack water because the travel time approaches infinity, whereas in the reversing macro-regions, survival increases near slack water as the distance traveled approaches its minimum value (Appendix 4B).

Together, the mechanisms of these behavior modules interact to produce realistic and well-explained migration and survival dynamics. The model incorporates behavioral dynamics that have been observed in juvenile salmon across numerous systems; however, every module might not be observed in every system. Thus, the model can be simplified by "turning off" a module by setting parameters to specific values. This is a strength that allows the model enough flexibility to emulate observed behavior in a given system (Table B.1).

4. Model calibration

We applied the *ePTM* to study migration through the Delta of Sacramento River-juvenile Chinook salmon. We calibrated the model by comparing the distribution of travel times and survival obtained from releases of acoustically tagged fish into the system and *ePTM* model simulations with matched simulated fish releases. To calibrate the model, we searched for optimal parameter values using a customized search process.

4.1. Calibration data

To calibrate the *ePTM* for salmonid migration in the Delta, we used data from tagging studies of Late Fall-run Chinook salmon (2006–2010) released in the Sacramento River (Perry et al., 2010). In total, 1591 tagged Late Fall-run juveniles were released in eight groups over the 5-year period (Table 2). These fish were tagged with VEMCO V5 acoustic tags and were tracked across multiple hydroacoustic receiver arrays (Fig. 2). Multistate Mark Recapture (MMR) models were fit within a hierarchical Bayesian framework to concurrently estimate detection, routing and survival probabilities through the different regions (Perry et al., 2010; Perry et al., 2018). In addition to the regional survival estimates, the data also included first detection times for each fish whenever it was detected at a receiver array. We fit the model parameters to the observed travel time distributions and MMR-estimated survival rates in each region.

4.2. Generating ePTM predictions for model calibration

In the *ePTM*, the model parameters can take different values in different parts of the domain. This allows us to capture spatial changes in behavior along simulated fish trajectories. To balance model parsimony with flexibility, we imposed the restriction that parameter values should be constant within each region. This does not preclude the possibility that some parameters may take on similar values across regions. In total, the 11 parameters in the *ePTM* (Table 1) can vary across the nine regions (Fig. 2), giving 99 model parameters that must be fit using the data.

To produce predictions from the *ePTM* for fish in the calibration dataset, we identified the first detection times of each fish detected in both the upstream and downstream ends of a region in the calibration data. For each of these fish, we released 10 simulated fish in an *ePTM* simulation for which the *DSM2* model was used to compute the flows over the migration period. The durations of these simulations were set to be ten days longer than the last initial detection time of fish at the downstream end of the region. For each tagged individual, the fate of each simulated migrant in the region as well as the travel time through the region was recorded. Simulated fish were introduced into the model domain at the same locations as the telemetry stations demarcating the upstream ends of the MMR regions. By performing such simulations over a large set of parameter values, a representation of the model goodness-of-fit to the data was obtained. This was used to estimate model parameters.

4.3. Model parameter constraints

Much data is available in the literature regarding animal swimming behaviors from which prior expectation can be set for the swimming parameters (Appendix C): $|\widetilde{u}_s|$, and $\sigma_{|u_s|}$ were restricted to a range of 0 to 0.5 m/s, and u_F to a range of 0 to 1.5 m/s (Table 1; Appendix C). We allowed p_M, $\widetilde{P}_{\text{Rheotaxis}}$, p_{DS} and p_H to vary between 0 and 1 (Table 1). The values of c and b were bound between –10 and 10, and 0 and 10, respectively (Table 1; Appendix C). We set the lower and upper limits for u_F to be 0 and 1.5 m/s, respectively (Appendix C). λ and ω were allowed to vary between 10 and 1,000Km, and 0 and 2 m/s respectively (Table 1; Appendix C). The survival parameter bounds were set based on the results in Perry et al. (2018) and simulations using a "*toy PTM*" model, which involved a very fast random walk of simulated fish with behaviors identical to the *ePTM* over three coarsely defined Delta regions (Appendix C).

4.4. Calibration process

To calibrate the model parameters with the Late Fall-run Chinook salmon data, we applied a custom 4-stage process (see Appendix D for details). First, we deduced that the movement (swimming, orientation and holding) parameters could be fit independently of the survival parameters (see below). Second, we performed a coarse grid search on a large number of movement parameter values to hone in on the best local

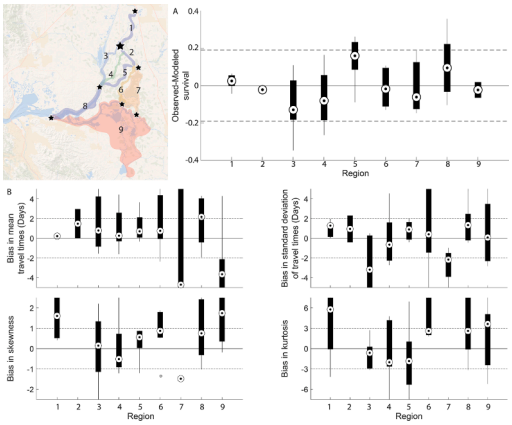

Fig. 4. Calibration performance: A. Deviation of predicted survival from observed survival measured as MMR-modeled – *ePTM* predicted survival. The boxplots include estimates of survivals for all release group using the best performing twenty survival parameter sets in each region. B. Biases between observed and *ePTM* simulated travel time distribution statistics for late-Fall run Chinook. Rows indicate release groups and columns indicate regions. In all the panels, a value of zero indicates a perfect match between observation and prediction. Dashed lines in A indicate deviation limits within which 95% of the model results fall. Dashed lines in B indicate the generally acceptable bias ranges within which the observed and modeled travel time distributions may be considered indistinguishable.

optima defined within a multiobjective optimization framework (Appendix D). Third, we performed a fine grid search in the neighborhoods of the best local optima obtained from the coarse grid search to identify the global optimum movement parameter values using the same optimization framework. Fourth, we held the movement parameters at their optimum values and performed a grid search over the survival parameters to find the optimum values of these parameters. We decided to use this custom approach due to a host of practical considerations, which we discuss further in Section 6 below.

For an 11-dimensional parameter space in each region of the model domain, space-filling algorithms provide an efficient way of sampling with significantly fewer points than a random selection of points which could fall on lower-dimensional manifolds. To select the optimal space-filling algorithm, we compared ten algorithms using the R package *DiceEval* (Dupuy et al., 2015). Using the maximum separation method with a minimum separation criterion of 0.244 produced the best performance out of all the approaches across four performance metrics (Appendix D). We compared the minimum separation criterion across 500, 5000 and 50,000 sets of parameter value combinations, or design points, and found that the criterion value was indistinguishable between 5000 and 50,000 design points. We then generated 5000 design points by sampling a standardized value of each parameter (by subtracting the mean of the parameter range and dividing by its range) from within the permissible range of values for that parameter using a maximum separation criterion-based space filling algorithm in the R package *DiceDesign* (Dupuy et al., 2015). The calibration dataset contained eight release groups, and survival and travel times could be computed reliably from these data for the nine regions. This yielded a total of $5,000 \times 8 \times 9 = 360,000$ *ePTM* model calls.

As MMR analysis had been performed for each region, we could fit the 11 model parameters for each region independently of the other regions. But within each region, to further reduce the complexity of fitting the 11-dimensional parameter set, we used the *toy PTM* model to identify whether any parameter simplification or decoupling was possible. To do this, we applied the Morris method of elementary effects analysis (Iooss and Lemaitre 2015) using the global optimization toolbox developed by Pianosi and Wagener (2015) to study the relationships between the model parameters and the distribution of travel times and survival rates in the three regions (Appendix E). The Morris method is an efficient screening algorithm to study parameter interactions for high-dimensional models, which allowed us to identify parameter interactions with just 3400 *toy PTM* model calls (Appendix E). Based on this analysis, we decoupled the model fitting process for the *ePTM* to first fit the nine movement parameters, and then fit the two survival parameters holding the movement parameters at their optimal values.

5. Results

Results of the *ePTM* calibrated for Chinook salmon migrating through the Delta show strong agreement with many of the major patterns evident in the acoustic telemetry data (see Appendix D for a detailed presentation). Moreover, parameter estimates reflect the behavioral patterns evident in our empirical analyses of data. These agreements between model and data suggest that (i) the *ePTM* is capable of capturing the salient features of salmonid migration through the Delta to make accurate predictions, and (ii) the module structures, assumptions, and interpretation of parameters are consistent with empirically observed behaviors of migrating fish in the system.

Except for $\sigma_{|u_S|}$, u_F, p_{DS}, and λ, the spread in the top twenty best performing parameter sets is very tight (Fig. D.2). The parameters with wide spreads were difficult to constrain as well as estimate from the data. In the case of the other parameters, the widest spread in the top performing parameter sets was observed in region 6 for b and p_M, where the flow is strong, but regularly reverses. So, it is not unreasonable that the parameters associated with the swimming orientation should be sensitive to the timing of fish releases in this region. Our λ and ω parameters are significantly larger than those typically reported in the literature (see Section 3.8). For example, while Steel et al. (2020) report $\lambda' \approx 100\text{Km}$ and $\omega' \approx 0.05\text{m/s}$, by applying Equations (A.6) and (A.8) with typical values of variance in water velocities in the Delta, we get equivalent values of $\lambda \approx 700\text{Km}$ and $\omega = 0.2\text{m/s}$. These values are of comparable magnitude with our calibrated optima.

5.1. Calibration results

The calibrated model accurately predicts travel time distributions and survival observed in the Late Fall-run Chinook salmon dataset. We show regional deviations of *ePTM*-predicted survival estimates relative to MMR-estimates in Fig. 4A, obtained by applying Eq. (8) to each simulated fish. Some regions show considerable variability in deviations between *ePTM*-predicted and MMR-estimated survival within-region (the regions of the Mainstem Sacramento River and the Sutter and Steamboat Sloughs in which the flow reverses tidally), whereas others are more consistent (the nonreversing regions of the Sacramento River and the Interior Delta). Nevertheless, in most regions, parameter estimates only vary by a factor of two to three (Fig. 4A). In general, predicted survival estimates are within ± 0.2 of MMR-modeled survivals throughout the Delta, indicating that the model can capture survival patterns across the diverse habitat and hydrologic conditions present in different regions of the Delta.

A second variable that can be predicted by *ePTM* is the distribution of migrant travel times. In Fig. 4B, we show the distributions across release group of biases between observed and predicted travel time distribution means, standard deviations, skewness and kurtosis coefficients in the different regions. The model predictions show strong agreement with travel time distributions for nearly all release by region combinations. Typically, the bias between mean travel times predicted by the model and the mean observed travel times is less than two days, except in regions 7 and 9, where only few tagged fish were left. However, simulated fish in the ePTM travel systematically slower than equivalent tagged fish. This is because of the 1591 fish used to calibrate the model 1028 were released during the four lowest flow periods in the calibration

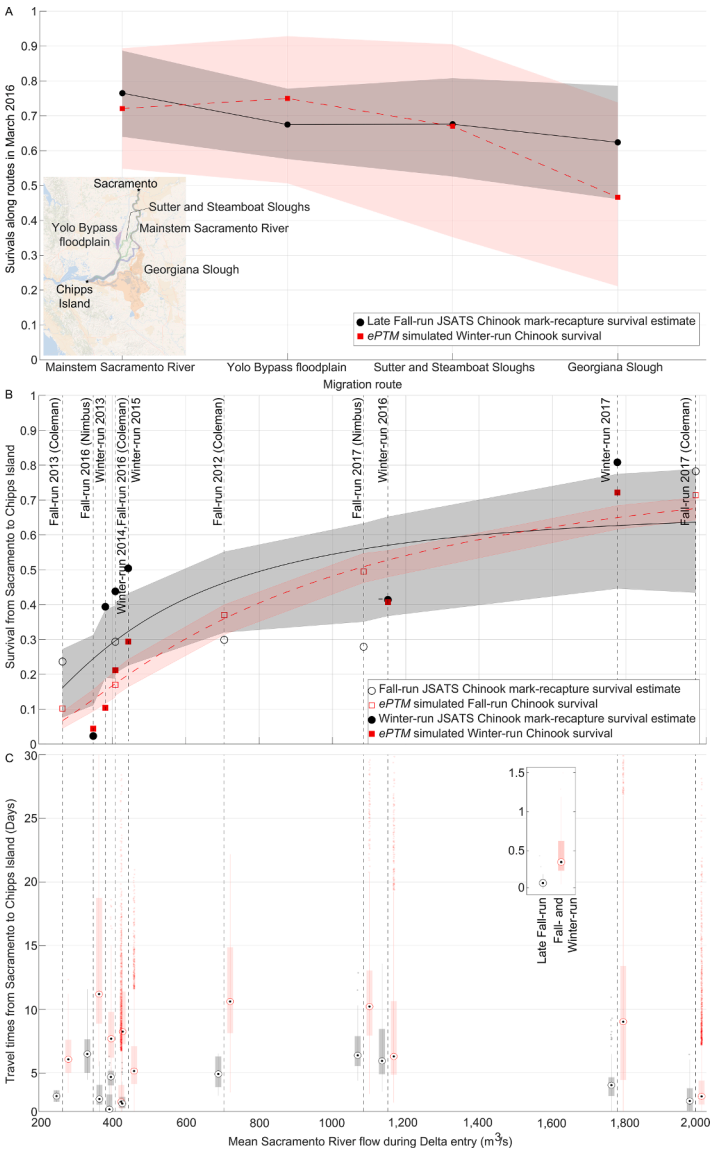

Fig. 5. Comparison between *ePTM* predictions and observed survival in out-of-sample data: A. along different migratory routes (indicated in the inset map) as reported Pope et al. (2021), and B. between Sacramento and Chipps Island. C. Distribution of travel times between Sacramento and Chipps Island for the datapoints and model results in B. Red squares and black circles respectively represent model predictions and MMR estimates fit to the data. Open symbols indicate Fall- and closed symbols indicate Late Fall- or Winter-run releases. For each release, flows were estimated as the mean flow in the Sacramento River at Freeport over the duration between the first fish passage and the last fish passage through this location. The dashed red line ($S = e^{-\frac{X}{258\text{km}}\sqrt{1+\frac{(1.225\text{m}^3/\text{s})^2}{Q^2}}}$) and black solid line ($S = e^{-\frac{X}{624\text{km}}\sqrt{1+\frac{(4.472\text{m}^3/\text{s})^2}{Q^2}}}$) represent an *XT* model fit to the model results and the MMR-reported survivals (functions indicated). Red and gray shaded areas represent 95% confidence intervals reported in Pope et al. (2021) and generated by bootstrapping 1000 replicate survivals in A., and generated by applying the same *XT* model fit to 1000 replicates of these points chosen at random with replacement in B. The overlap of these confidence intervals indicates that the model precision is up to data precision. The lower survivals in B. and longer travel times in C. predicted by *ePTM* can be attributed to the significantly faster migration rates relative to water velocity by the much smaller Fall- and Winter-run Chinook with which the model was validated compared to the larger and slower-moving Late Fall-run Chinook with which the model was calibrated (inset boxplot in C). In A, the route-specific MMR-reported survivals of Late Fall-run Chinook are compared with *ePTM* predictions. In B and C, the overall MMR-reported survivals and observed travel time distributions of Fall- and Winter-run Chinook are compared with *ePTM* predictions.

dataset. This imbalance in the data has likely biased the model to predict smaller movement parameters, as the larger number of fish would have skewed the goodness-of-fit measures, particularly in regions away from the mainstem Sacramento River. The variation of the predicted standard deviation in travel times and the actual standard deviation in travel times is typically less than two days. For migrations through regions that typically take a few days, these deviations are quite small. The biases in skewness and kurtoses generally fall within ± 1 and ± 3 respectively, indicating that the observed and modeled travel time distributions are not significantly dissimilar in shape from each other. However, in regions 1, 5, 6 and 9, the model failed to reproduce multimodalities in the travel time distribution. This pattern may be due to differences between individual fish that the model does not attempt to capture. Nevertheless, on the whole, the model is able to simulate survival and movement dynamics through the Delta.

5.2. Out-of-sample validation

To validate the model, we selected fourteen releases of hatchery-reared Juvenile Salmon Acoustic Telemetry System (JSATS)-tagged Fall-, Late Fall- and Winter-run Chinook salmon between 2012 and 2017 (J. Notch et al. 2021; Pope et al., 2021) in which 2052 fish entered Delta at Sacramento (Table 3). These data were obtained from the California enhanced acoustic tagging project, which provides arrival data and MMR survival estimates (Notch et al., 2020; J. 2021). We used data from release groups that met two criteria: (i) at least 100 fish were released, and (ii) the fish were observed at least at the telemetry stations at the landward and oceanward (Chipps Island) ends of the Delta. The validation dataset comprises of different runs of Chinook salmon than the calibration dataset, as well as encompasses different flow regimes (260–2150 m^3/s versus 360–760m^3/s in the calibration dataset), and different fish forklengths (84–168 mm versus 150–166 mm in the calibration dataset).

Survival predictions along different migratory routes for out-of-sample releases were produced by releasing 50 simulated fish at *DSM2* nodes within each migratory route (inset map in Fig. 5A), applying Eq. (8) to each individual, averaging across all individuals released in each migratory route, and subsequently averaging across the three releases reported in Pope et al. (2021) weighted by the number of fish in each release (Table 3). Overall survival predictions from Sacramento to Chipps Island for each release were obtained by releasing ten simulated fish for each real fish released, applying Eq. (8) to each individual, and averaging across all individuals released. In these validation studies, the model parameters in each region were set to their optimal values.

Table 3
Details of the validation dataset.

S. No.	Validation test	Run	Period of Delta entry	Mean flow during Delta entry (m^3/s)	Number of fish at Delta entry	Mean forklength of fish (mm)
1	Through-Delta survival	Fall	24 Apr.–8 May 2012	705.1	18	84.9
2	Through-Delta survival	Fall	15 Apr.–6 May 2013	264.4	49	84.2
3	Through-Delta survival	Fall	12 Apr.–10 May 2016	408.3	54	84.0
4	Through-Delta survival	Fall	9 Apr.–6 May 2017	1989.9	118	82.4
5	Through-Delta survival	Fall	15–19 May 2016	348.1	220	89
6	Through-Delta survival	Fall	25 May–4 Jun 2017	1084.9	204	85.6
7	Through-Delta survival	Winter	3 Mar.–1 Apr. 2013	381.1	10	98.6
8	Through-Delta survival	Winter	19 Feb.–23 Mar. 2014	408.4	121	96.1
9	Through-Delta survival	Winter	9 Feb.–16 Mar. 2015	443.5	157	101.7
10	Through-Delta survival	Winter	22 Feb.–22 Mar. 2016	1151.2	278	96.4
11	Through-Delta survival	Winter	10 Mar.–7 Apr. 2017	1776.3	106	95.1
12	Survival by migratory route	Late Fall	11 Mar.–12 Mar. 2016	1849.9	240	167.2
13	Survival by migratory route	Late Fall	15 Mar.–16 Mar. 2016	2147.6	240	166.1
14	Survival by migratory route	Late Fall	17 Mar.–18 Mar. 2016	1996.0	237	168.9

The route-dependent survival estimated by the *ePTM* captures the general trend of higher survival along the Mainstem Sacramento River and North-Delta Sloughs, and reduced survival in the Interior Delta (Fig. 5A). 95% confidence intervals on the survivals reported in Pope et al. (2021) and those predicted by the *ePTM* overlap one another, indicating that the model precision is comparable to that of the MMR estimates.

In Fig. 5B, we show MMR-estimated and predicted survival of Chinook salmon passing through the Delta as a function of mean flow in the Sacramento River. The flow-survival relationship is a crucial tool that aids in overall management of water resources as it gives decision makers an understanding of what levels of flow must be maintained for providing essential ecosystem services. So, a reliable decision support model should be able to reproduce this relationship. We fit a Delta-wide *XT* model to the MMR-estimated and predicted survivals (see Appendix D) to evaluate whether *ePTM* is able to reliably represent this relationship. The model follows from Eq. (8) as

$$P(\text{Survival}) = e^{-\frac{X}{\bar{\lambda}}}\sqrt{1+\frac{(\bar{A}\omega)^2}{Q^2}} \tag{9}$$

Here, $\bar{\lambda}$ and $\bar{A}\omega$ are fitting parameters which represent a Delta-wide lengthscale of survival decay and a flow scale respectively, $X = 99.2$ Km is the distance between Sacramento and Chipps Island along the Sacramento River, and Q is the mean river flow during Delta entry by fish. The fitting parameters we obtained were $\bar{\lambda} = 258$Km and $\bar{A}\omega = 1,225\text{m}^3/\text{s}$ for the MMR-based survival estimates, and $\bar{\lambda} = 624$Km and $\bar{A}\omega = 4,427\text{m}^3/\text{s}$ for the survivals predicted by the *ePTM*. The discrepancies in these parameters may be attributed to systematic biases in the MMR estimation process and biological mechanisms not represented in *ePTM*. However, both parameter sets have the same orders of magnitude and result in similar shapes for the flow versus survival relationship.

ePTM predictions capture the major patterns evident in data. Firstly, through-Delta survival predictions of the model (red squares in Fig. 5B) are similar to MMR estimates from data (black circles in Fig. 5B). In most cases, the survival prediction is within 0.2 of the observed survival, although there is a bias towards lower survival when flows are low. This is likely because the Late Fall-run Chinook datasets used to calibrate the model were based on larger and slower moving fish than the smaller and faster moving Fall- and Winter-run Chinook datasets used for validation (Tables 2 and 3 and inset boxplot in Fig. 5C), resulting in slower migrations in the *ePTM* than in the data (boxplots in Fig. 5C). This could also be because of the mean-field treatment of mortality using the *XT* model. When flows are low, the water column is generally clearer, and so migrants might be able to see predators earlier and avoid being eaten (Martin et al., 2021). As the *XT* model within the *ePTM* has been calibrated using typical flow conditions, such nuances will not be represented in the model. Overall, the model reproduced the shape and scale of the observed relationship between survival and mean river flow through the Sacramento during migration through the Delta (lines and confidence intervals in Fig. 5B).

Another aspect of out-of-sample validation is model performance in predicting migration routing. To study how the model performs in predicting out-of-sample route use by salmon through the system, we selected those releases (2014 and 2015) of the JSATS program in which the endangered Winter-run Chinook salmon passages were recorded through two key junctions along the Sacramento River: the mainstem Sacramento River with Sutter and Steamboat Sloughs, and Georgiana Slough. A fish guidance structure was in place in 2014 at the head of Georgiana Slough with an overall passage efficiency of $\eta = 0.777$ (R.W. DWR 2016). This was represented in the model as a synthetic barrier with the same efficiency. Results are shown in Fig. 6, which shows observed and predicted salmon detected along different possible routes at the two junctions. To see if the model is able to reproduce routing during different phases of the tide, we stratified this comparison by phase of the tide, defined at the junction with Sutter and Steamboat Sloughs with respect to the flow reversal in Steamboat Slough, and at the junction at Georgiana Slough with respect to the flow reversal in Georgiana Slough. In both years, the model is able to predict the qualitative patterns in the data correctly, and quantitative routing probabilities to within ±20% from the observed values, which is notable, given that observed routing is not used to calibrate the model.

5.3. Behavioral implications of optimal parameter values

Estimates of model parameters are shown for each Delta region in Fig. D.2. In Fig. D.3, we show how the optimal parameter values for each process within the *ePTM* evolve through a simplified schematic network representation of the Delta. The combinations of these parameter values in the *ePTM*'s behavioral modules results in migration patterns that are consistent with the data collected in the Delta (Fig. D.4).

For the active swimming component of the model, the values of $|\bar{u_S}|$

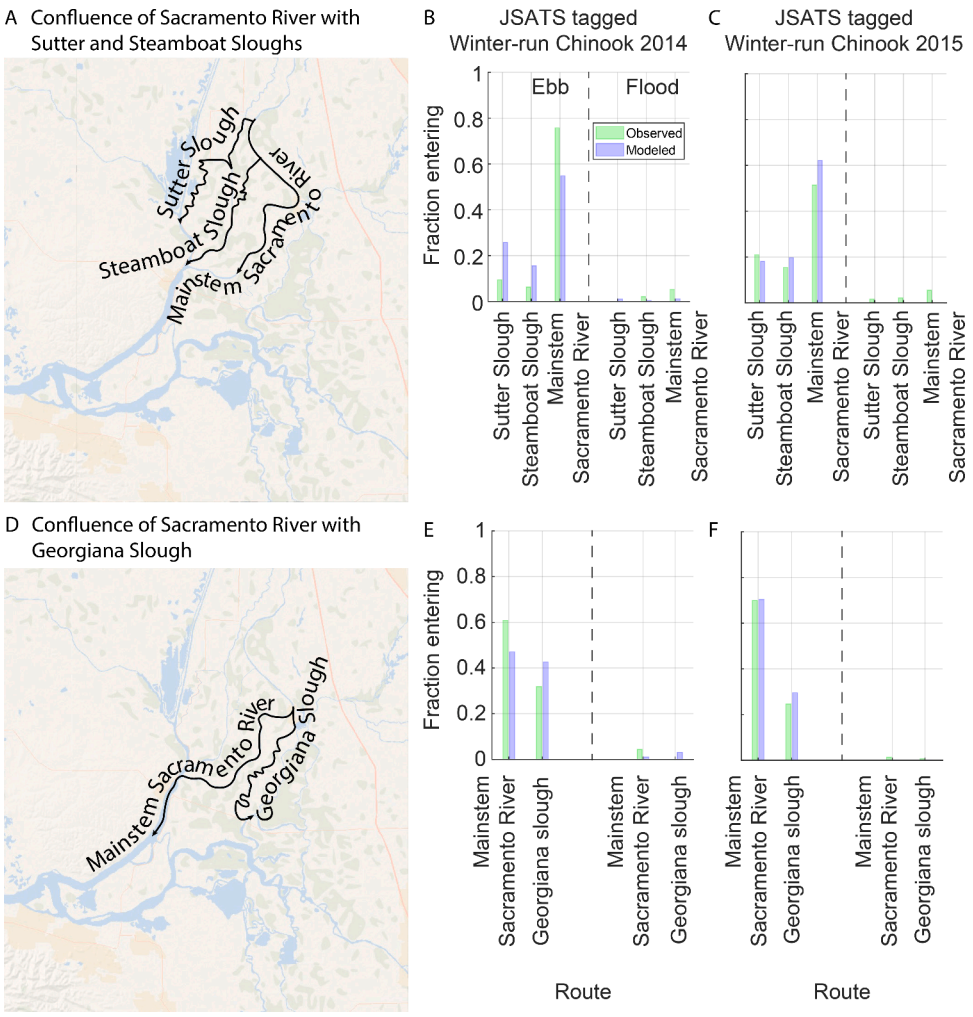

Fig. 6. Comparison between *ePTM* predictions and observed route use in out-of-sample data. A. and D. indicate routes studied. B. and E., and C. and F. indicate comparisons respectively in 2014 and 2015. Green bars indicate fraction of total Chinook passing through telemetry stations in the different routes. Blue bars indicate *ePTM* predictions of fraction of particles passing through equivalent nodes on the *DSM2* grid. Passage fractions are aggregated over different phases of the tide at two key junctions that are important to overall survival in the Delta: the Mainstem Sacramento River with diversions to Sutter and Steamboat Sloughs on the left, and the Mainstem Sacramento River and Georgiana Slough on the right. In both out-of-sample years, the patterns of route use observed in the data are predicted reasonably well by the model. In E, in 2014, a floating fish guidance structure was in place upstream of Georgiana Slough, and this has been represented in the model with a barrier efficiency of 77.7% reported in R.W. DWR (2016).

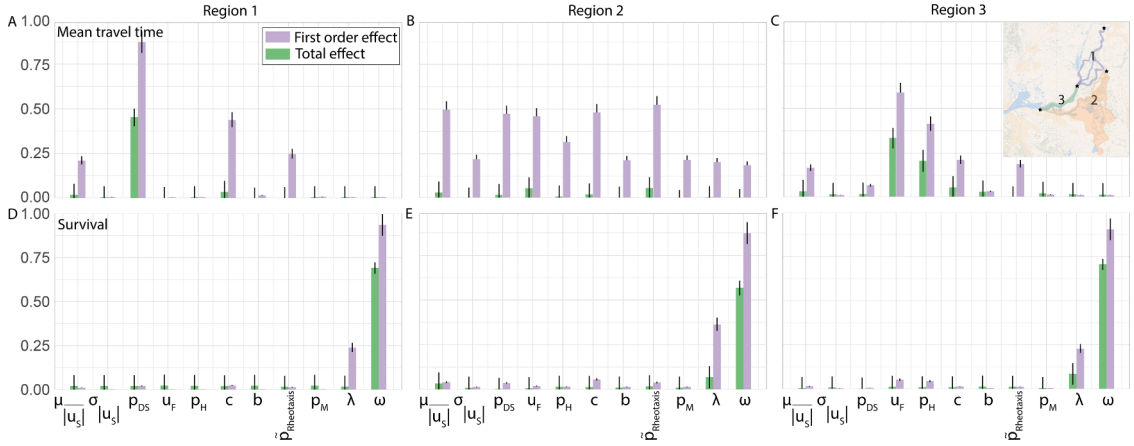

Fig. 7. Global sensitivity analysis of the *toy PTM* using first order and total order Sobol indices. A.-C. Sobol indices with respect to the mean travel time. D.-F. Sobol indices with respect to the survival rates. The size of the bars indicates the contribution to the variance in the model results, while the error bars indicate confidence intervals about the estimates of the Sobol indices. Region numbers correspond to those shown in the inset map.

decrease from 0.44 m/s in the nonreversing macro-region to 0.36 m/s in the tidally reversing macro-regions, and $\sigma_{|u_S|}$ increase from 0.85 m/s to 0.97 m/s. The large values of $|\bar{u_S}|$ combined with small values of $\widetilde{P}_{\text{Rheotaxis}}$, and large p_Ms in the nonreversing macro-region result in simulated fish actively swimming against strong nonreversing flows. In the more tidally reversing macro-regions, decreasing $|\bar{u_S}|$, increasing $\widetilde{P}_{\text{Rheotaxis}}$ (typically exceeding 0.5) and reduced p_M result in simulated fish executing either movements that are directed weakly with or against the flow (Fig. 3C). $\sigma^2_{|u_S|}$ generally increases with proximity to the ocean. Together, these parameters result in actions by the simulated fish that increase migration rate and dispersion with proximity to the ocean, as we observed in the acoustic telemetry datasets (Figs. 3B and E.4).

Table B.1
Behavior models with simpler model formulations.

Behavior module	*ePTM*	Simpler functional form	Constant value	Off
Active swimming	Migration rate and dispersion vary across space.	Coupled migration rates and dispersion.	No variability in swimming speeds within and between individuals.	Passive particles drifting with the flow.
Orientation	Shifts in movement mechanisms with proximity to the ocean.	Reduced sensitivity to flow conditions.	No shifts in movement mechanisms with proximity to the ocean.	Dispersal attributed to unexplained dispersion.
Holding	Observed patterns of holding during the day time and against the incoming flood tide.	No spatial variability in migration behavior.	No holding as a function of flow or day/night cycle	Migration rates and dispersal attributed to unexplained fitting parameters.
Mortality	Spatial patterns in survival.	Single predatory type.	No spatial heterogeneity in mortality.	No mortality.
Routing	Realistic route use.	Flow-based randomized routing.	Fixed route use.	Individual routes modeled separately.

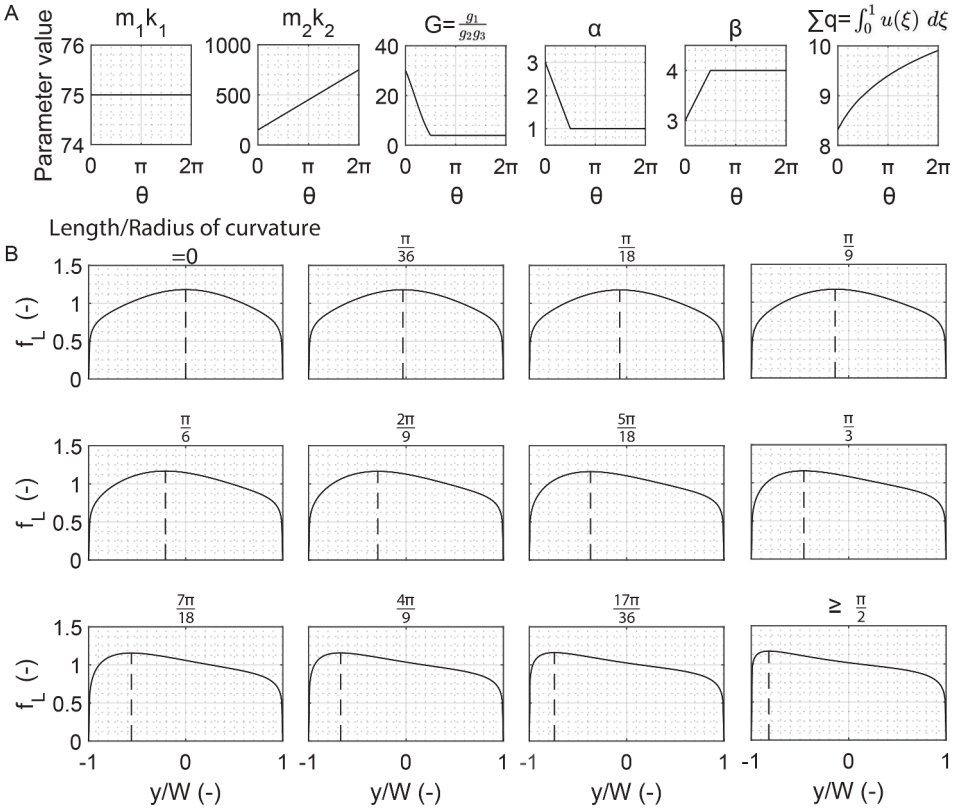

Fig. A.1. Lateral profiles of the streamwise water velocity obtained by Gandhi et al. (2016) in flume experiments. A. fitted parameter values as a function of bend angle. B. Normalized water velocity profiles for various bend angles.

The orientation and holding parameters allow simulated fish to hold against the flow, and even swim against the flow during the landward flood phase of the tide (Fig. 3D). The trends in c and b are both decreasing through the Delta. In the nonreversing macro-region, the net effect of these parameters in combination with the small values of $\widetilde{P}_{\text{Rheotaxis}}$ is to orient simulated fish against the flow much more often than with the flow. In the parts of the system where the flow reverses tidally, these parameters allow the logistic response to be small when flows are weak, and thereby result in simulated fish orientations that may switch between with and against the flow. In the reversing macro-regions, when flows are strong and oceanward, the combination of c, b and $\widetilde{P}_{\text{Rheotaxis}}$ allows simulated fish to be oriented more often with the flow. During strongly landward flow reversals, which are quite rare under historic conditions (Fig. 3A), u_F and values $p_H > 0.5$, result in simulated fish approximately maintaining position. p_{DS} is around 0.5, with no appreciable trend through the system, which is consistent with the values between 0.34 and 0.75 obtained in this region from acoustic telemetry experiments reported in Chapman et al. (2013). Together, these holding mechanisms contribute to fish typically holding about 75% of the time throughout the system (Fig. 3D).

λ generally increases through the system, while ω decreases. In the Delta, predators are distributed largely in the fresh Sacramento and San Joaquin River waters than in the saltier Western part of the system (Michel et al., 2020). The spatial distribution of the λ and ω parameters thus represent a lower likelihood of predation in the Western Delta than in the Eastern Delta. These patterns in λ and ω result in an overall increasing per-timestep likelihood of survival through the tidally reversing macro-regions. However, it typically takes significantly longer to move through these reversing flows, and so the overall survival through these macro-regions is lower than through the nonreversing macro-region (Fig. 3E).

5.4. Sensitivity analysis

To evaluate the sensitivity of model predictions to parameter values, we performed a Global Sensitivity Analysis (GSA) with a quasi-Monte Carlo Analysis Of Variance (ANOVA; Owen 2013) decomposition of the variance in mean travel time and survival using the R package

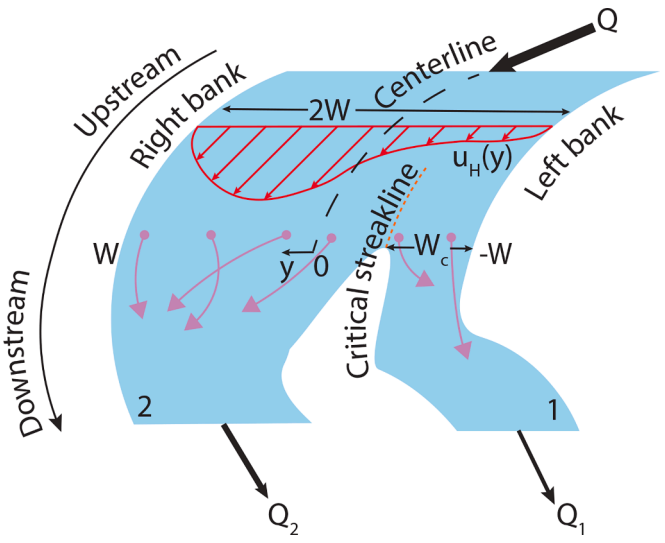

Fig. A.2. Schematic routing of simulated fish (pink dots and arrows) through a channel junction depending on their lateral position [driven by the water velocity profile, $u_H(y)$ (red arrows)] relative to the critical streakline at distance W_c from the left bank looking from the upstream end (dotted orange line) in the inflow channel of width $2W$. The flows entering and exiting the junction dictate the location of the critical streakline. The location of the inflow channel centerline is also shown for completeness.

Sensitivity (Iooss 2021). Briefly, the ANOVA decomposition allows the variance in the model results to be expressed as a sum of the contribution of the conditional variance associated with each parameter (or the first order effect of that parameter) and the conditional variance of two-, three-, and up to n-way parameter interactions. This decomposition can be rewritten efficiently for each parameter into its first order effect, and the sum of the variance of all its interactions with other parameters (its total effect). For the ANOVA decomposition, we used Sobol indices. Sobol indices are the first and total order effects estimated using $K{\cdot}(n+2)$ model calls at sequentially perturbed parameter values (Baudin et al., 2016; Appendix E).

To evaluate the sensitivity of the model to parameters in a computationally tractable manner, we used the reduced-complexity *toy PTM*. Since the structure of the two models is identical and they are both driven by real flows, with the only difference being the simplification of the *toy PTM*'s model grid, we expect the sensitivity of either model to the parameters to be very similar. We performed $1,000 \times [3 \times (11+2)] = 39,000$ model calls independently over the three regions to compute the Sobol indices in Fig. 7.

We observe that in the regions upstream of Georgiana Slough where the flow does not usually reverse (Fig. 7A corresponding to region 1 in the *toy PTM*), the modeled travel times are likely most sensitive to p_{DS}, c, $\widetilde{P}_{\text{Rheotaxis}}$, and $|\bar{u_S}|$ (the parameters with the strongest first order effects). The model is relatively insensitive to b and $\sigma_{|u_S|}$, here owing to the strong oceanward currents and low observed dispersal of fish in this region.

In Georgiana Slough, the Delta Cross Channel and the Interior Delta (Fig. 7B corresponding to region 2 in the *toy PTM*), we observe that the interactions of all the parameters contribute significantly to the sensitivity of the travel time simulation. This is because of the tidally reversing flows and complex topology in this region that cause emergent behaviors that vary in response to flow and behavioral memory. The sensitivity to b in this region indicates that the shape of the logistic function, which dictates the rapidity of the response to changing flows is important here. The dependence of the mean travel time to the survival parameters in this region only occurs through the interaction of these parameters with the movement parameters, and the total effects associated with these parameters are the lowest amongst all the parameters. Thus, our decision to decouple the movement and survival parameters during model calibration based on the elementary effects analysis of the results of the *toy PTM* is justified.

In the Southwestern region of the mainstem Sacramento River (Fig. 7C corresponding to region 3 in the *toy PTM*), the travel time simulations are most sensitive to u_F, p_H, c, $|\bar{u_S}|$ and $\widetilde{P}_{\text{Rheotaxis}}$. In this region, the dispersion of fish in the acoustic tagging data is large, and therefore the model is insensitive to values of $\sigma_{|u_S|}$. However, as the flow strongly reverses here, simulated fish behaviors will be highly sensitive to assumptions about the holding and rheotaxis.

In all the regions, the modeled survivals are primarily sensitive only to λ and ω (Fig. 7D–F). Thus, the patterns revealed in the GSA indicates that the algorithms in the *ePTM* result in behaviors that were anticipated from the system-wide acoustic telemetry and high-resolution fish tracking data.

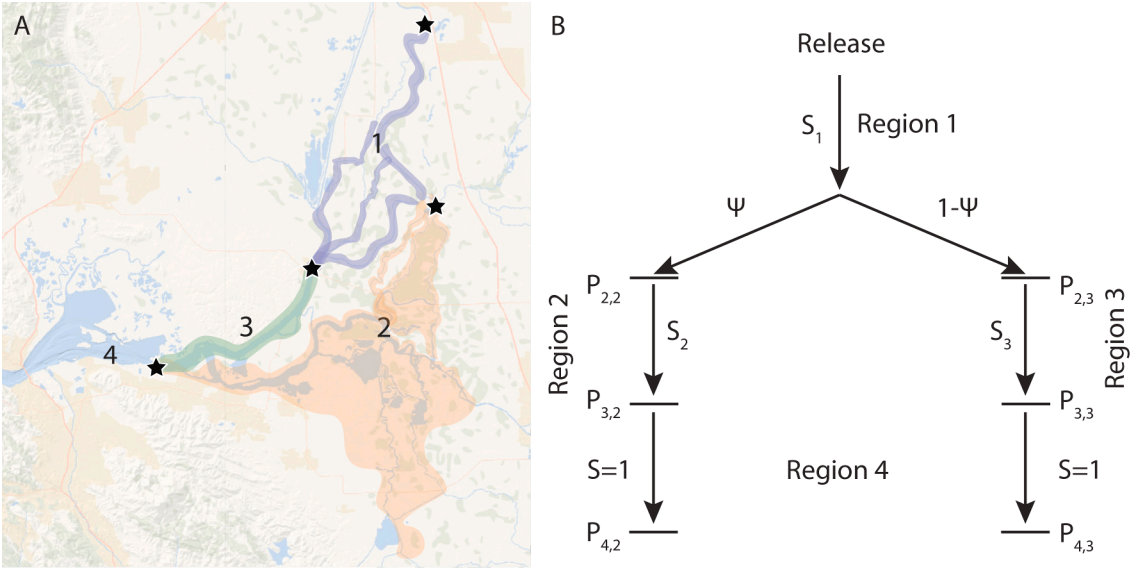

Fig. C.1. Schematic of channel structure and associated MMR model parameters for the *toy PTM*. The idealized grid in B corresponds to the regions in the map in A. Region 4 is used solely to provide detection stations within each route, and no particles are simulated there.

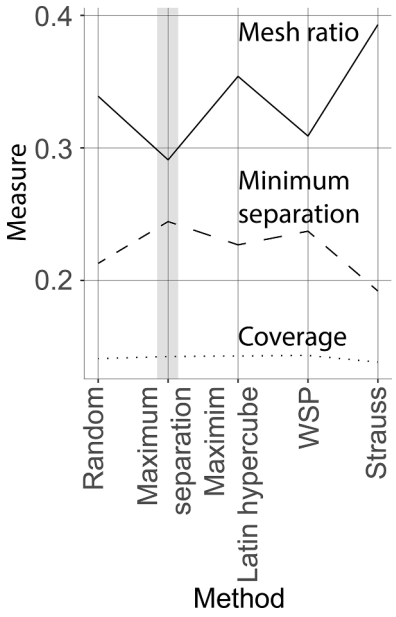

Fig. D.1. Selection criteria for candidate space-filling approaches. The values of mesh ratio (higher is better), minimum separation (higher is better) and coverage (lower is better). All selected candidate algorithms produced 11-dimensional points with satisfactory clumpiness. The maximum separation criterion was selected (shaded box) based on its overall performance across the four volume occupancy measures.

6. Discussion and conclusions

We have developed a data- and theory-driven agent-based model of juvenile salmonid migration through rivers and estuaries that incorporates behaviors observed in the literature and in field studies. This model allows simulated fish to move as a function of local flows and behavioral responses to environmental cues and memory of past actions. When calibrated for the Delta, the model accurately reproduces the survival and routing patterns of multiple runs of Chinook salmon, as well as the flow-versus-survival relationships. The flow-versus-survival relationship is a key water management metric used to plan operations such as pulsed dam releases for salmonid outmigration and diversions for agriculture, industrial and municipal use.

Given the complexity of behaviors observed in salmonids migrating through estuaries, the *ePTM* is a reasonably parsimonious model. The combination of the optimized spatially variable set of behavior modules produces environment-dependent behavioral responses that shift between the nonreversing and reversing flow macro-regions of the Delta (Fig. 3), resulting in migration and survival patterns that reproduce observations in both in-sample (Fig. 4) and out-of-sample (Figs. 5 and 6) datasets. The runs of Chinook and the seasons and flows that correspond to the calibration and out-of-sample validation are different for the calibration and validation. The validation, thus indicates that the mechanisms in the *ePTM* are indeed simulating salmonid migratory movements with high fidelity.

In the *ePTM*, the relative importance of parameters can vary spatially as the mechanisms underlying the physical movement of fish change. Both the Morris screening analysis (Fig. E.1) and the Sobol indices-based GSA with the *toy PTM* (Fig. 7) revealed similar parameter dependencies. These analyses qualitatively confirm that the model is able to represent the mechanisms of fish movement outlined in Section 2. Animal movements predicted by the model are most sensitive to swimming, memory, and local flow-based response parameters and their interactions in the nonreversing regions, and to more complex interactions of parameters in the tidally reversing regions in the Delta. Mortality is most sensitive to the interaction between the survival parameters. The interaction of the active swimming, orientation, holding, routing, and mortality elements thus produce emergent spatial patterns in the behavior that were not explicitly assigned *a priori*.

Calibrating the model exposed many challenges in optimizing complex stochastic agent-based models. We considered several established calibration methods before developing the pipeline used here. These included particle swarm optimization (Poli et al., 2007), emulation of the model predictions in conjunction with a Monte Carlo Markov Chain (MCMC) approach (Dancik et al., 2010), and sequential Monte Carlo with approximate Bayesian Computations (Scranton et al., 2014). Based on simulations using the *toy PTM*, we estimated that particle swarm optimization and approximate Bayesian methods would require twenty to thirty million model calls to converge. MCMC approaches would also require multiple chains of millions of model calls, necessitating the use of an emulator, The high dimensionality of the model made emulator construction challenging. The workflow we have developed here is comparatively tractable, and allowed us to arrive at the vicinity of the global optimum of parameter values with fewer than one million model calls. We could not compute empirical confidence bounds about the optimal parameter values, as this would have required at least one order of magnitude more model calls. The corroboration between the spatial trends in the model parameters (Figure E.3), functional responses of the behavior modules to flow (Fig. 3) and observed statistics of migration (Figure E.4), and the biologically plausible interactions among model parameters indicated in the GSA (Fig. 7), together help build confidence in our estimates of the parameter values.

There are two difficulties in the model calibration which we could not overcome. Together, these likely result in increasing modeled travel times and decreasing modeled survival compared to the data. The first is that the calibration data was skewed disproportionately towards a greater number of fish released during lower flows (Table 1). This meant that a greater number of fish also survived to the Interior Delta during these low-flow periods. Thus, the parameter space searched was also influenced by these low flow conditions. Second, the fish that the model was calibrated with were significantly larger than the fish that it was validated against (Tables 1 and 2 and inset in Fig. 5). In the Delta, the smaller fish migrate much faster relative to flow than larger fish (inset in Fig. 5). Together, these two factors resulted in smaller movement parameter values than real fish are likely exhibiting, longer travel times, and hence reduced survivals. At the time of model development, the Late Fall-run Chinook salmon datasets were the only ones available to us. In future iterations of the model, this imbalance in the calibration will be addressed.

There are some limitations in the biological component of *ePTM* which should be addressed in the future. Scaling arguments have been proposed for optimal and maximum cruising speeds of migratory aquatic animals that are theoretically limited by their body sizes and environmental conditions (e.g., Videler and Nolet 1990; Floryan et al., 2018). These bioenergetic constraints are not currently incorporated in the model explicitly. From Fig. 5C, it is evident that size-based movement speeds are likely to play an important role in improving travel-time distribution fits and hence, survival predictions. The lateral movements of fish are very likely independent of the turbulent motions in the flow, making the zeroth order turbulence closure model used in the *ePTM* to stochastically move simulated fish laterally unrealistic. For example, Kjelson et al. (1982) reported that juvenile Chinook in the Delta are typically found near the shore during the day and offshore at night. More recently, Goodwin et al., rev.) have reported that some Chinook salmon migrating in the Sacramento River exhibit zig-zagging trajectories which move from one bank to the other, while others move relatively quickly along the stream centerline. These types of studies indicate that individual migrants are heterogeneous. It is also possible for different individuals to school and interact. Such inter-individual heterogeneity and interactions, if captured in models like the *ePTM*, may result in superior model performance than the ergodic assumption that all individuals are alike and differences in behavior are purely aleatory. However, care

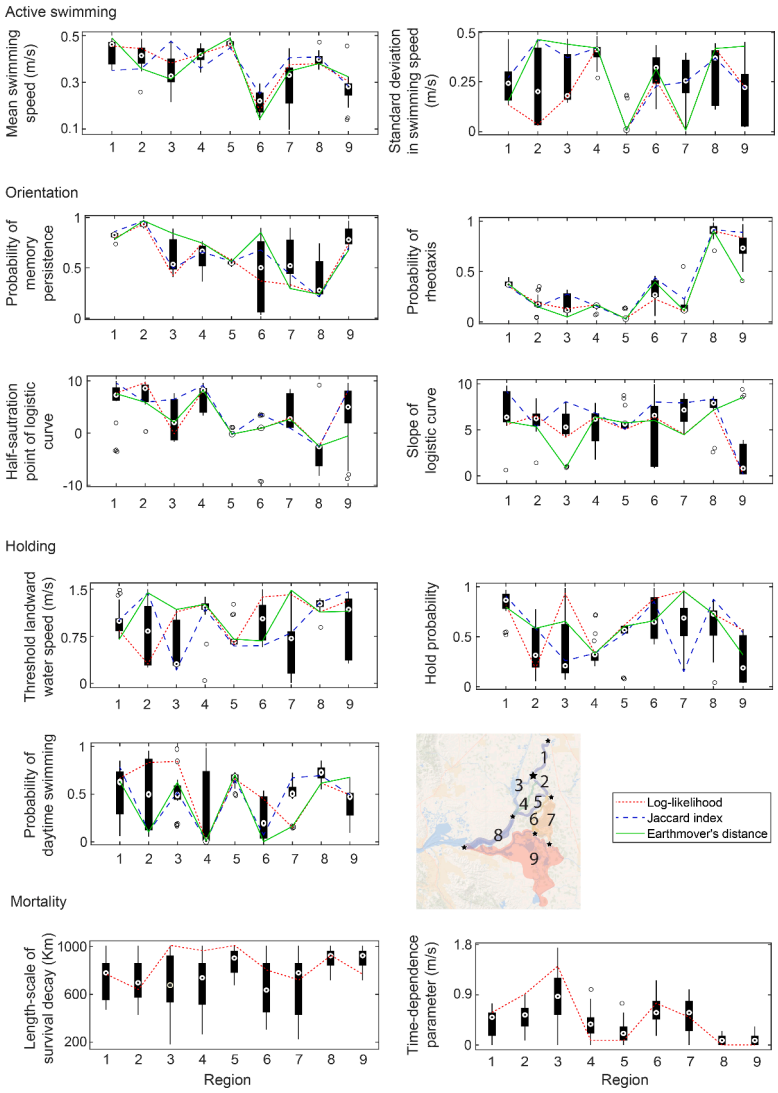

Fig. D.2. Spread in the top 20 best performing model parameter values in each region. For the swimming, orientation and holding parameters, the best performing model parameters for each of the three goodness-of-fit measures is shown using the lines. For the mortality parameters, the best performing model parameters in each region is shown using the solid lines. Region numbers correspond to those shown in the inset map.

must be taken in constructing a generalizable biological random walk model for lateral and vertical movements, owing to considerable ambiguity in the literature regarding the vertical placement of salmon within the water column (Azevedo and Parkhurst 1957; Mains and Smith 1964; Brett 1971; Smith 1974; Borthwick and Corwin 2001; Rundio et al., 2017), and lack of adequate vertical resolution in the acoustic telemetry studies.

Our application of the *XT* model of predation has some limitations. First, for fish that enter open water bodies, mortality is not estimated during the time they are in such areas. In places such as the Interior Delta, where there are many submerged islands with a few entry points due to breaks in levees, these open water areas may represent predation hotspots which are not represented in the *ePTM*. This could be the cause for the large deviation between modeled and observed survival in the Georgiana Slough route (Fig. 5A). Second, while migrants are actively attempting to avoid predators, predators are also trying to optimize their positioning within the water column and are responding to prey movements to maximize their likelihood of catching their prey. These dynamic interactions are not represented in the model and can be implemented in the future via a game theoretic formulation in which the ω parameter could be optimized by minimizing the differences between the outcomes of games played between archetypical predators and prey and observed survival rates in different parts of the system.

The three-dimensional water velocity and mixing profiles described in Section 3.2 allow for the general application of the model. However, for targeted applications to specific river and estuary systems, we recommend developing lookup tables using measured acoustic Doppler current profiler velocity and turbulent stress profiles to replace the laboratory-derived profiles of Gandhi et al. (2016). Similarly, the lateral stochastic turbulent movement rules can be readily modified to include more realistic biological random walks or nonparametric models (e.g., Olivetti et al., 2021; Gross et al., 2021). As long as the hydrodynamic model outputs are produced in a format readable by the *ePTM*, the model can be coupled with more sophisticated two- and three-dimensional flow models.

The *ePTM* is both a scientific tool and decision support model. As behaviors can interact with flow within the modular code environment, it is relatively straightforward to interchange behavior modules and hydrodynamic routines. For example, apart from the behaviors elaborated in Section 3, we also tested a suite of other behaviors, such as requiring simulated fish to (i) always swim towards the ocean, (ii) always swim near the water surface, (iii) swim only during the oceanward ebb phase of the tide, and (iv) swim in the direction of the positive salinity gradient. Thus, the model can serve as a numerical test bed for

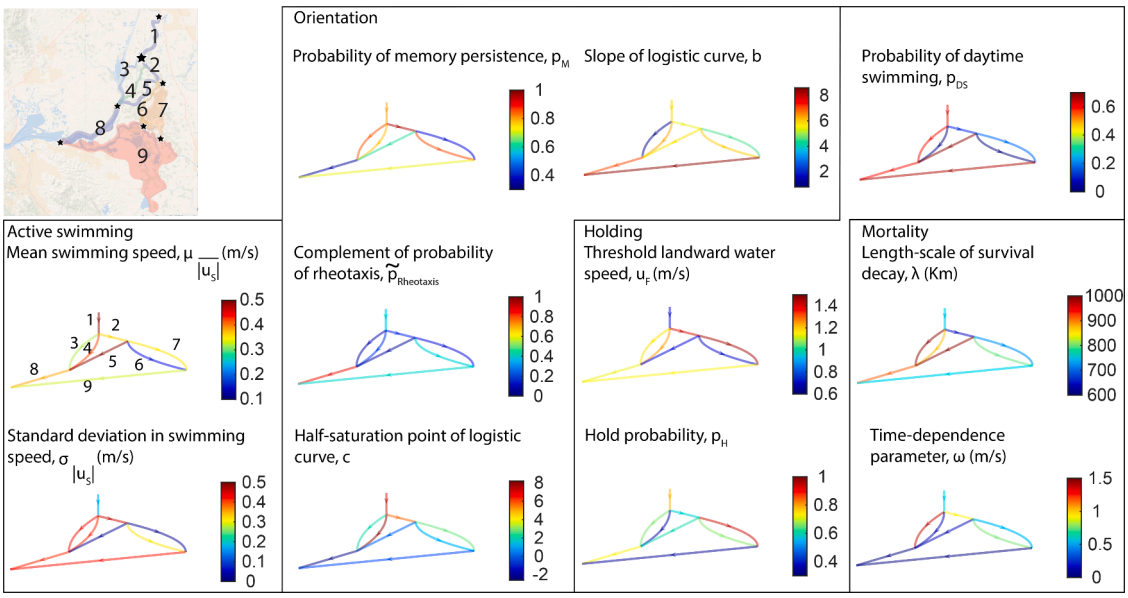

Fig. D.3. Parameter estimates across Delta regions. Schematic graphs of the Delta regions are color coded by the optimal parameter values. Region numbers correspond to those shown in the inset map.

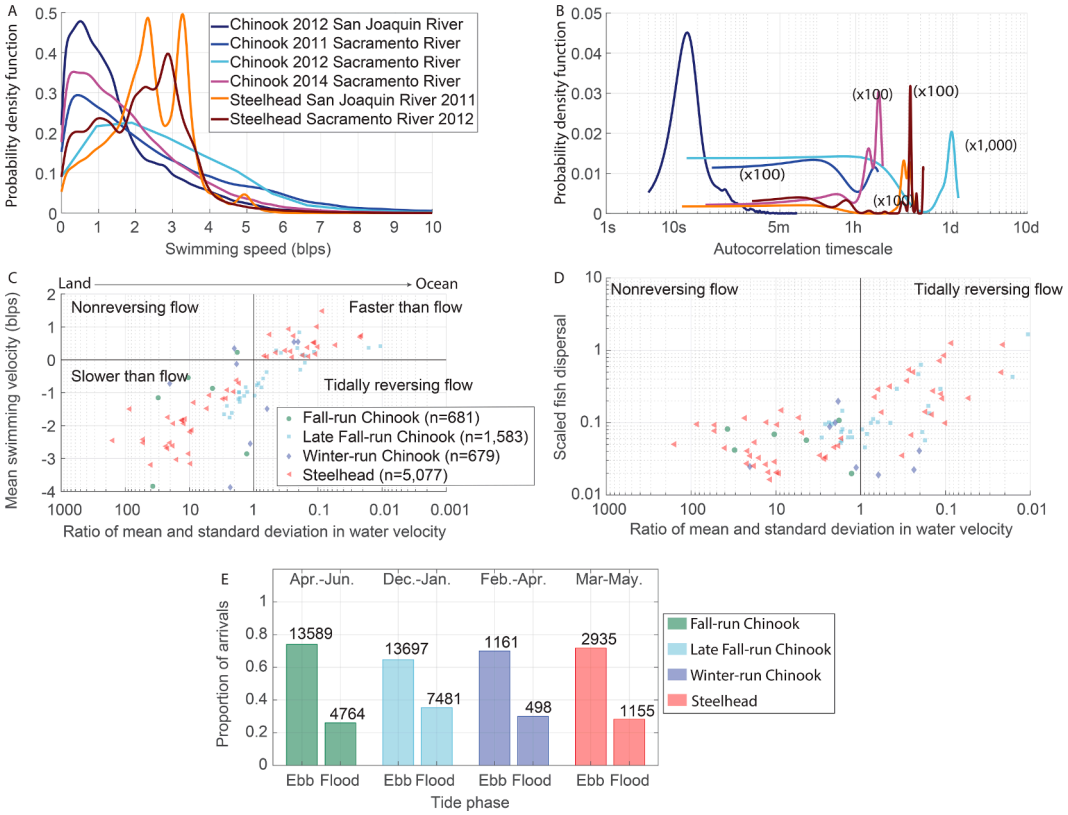

Fig. D.4. Data on salmonid migration through the Sacramento-San Joaquin Delta. For different salmonids observed in the high-resolution fish tracks, A. distributions of along-stream swimming speeds relative to flow, and B. autocorrelation timescales. For different salmonids observed in the large-scale acoustic telemetry studies, C. migration rate relative to mean flow changes from being directed against the flow to being directed with the flow as fish move oceanward and the strength of the mean current relative to the tidal fluctuations decreases, D. overall dispersal in fish increases as fish move oceanward, and E. fish arrivals significantly more frequently during ebb tides than during flood tides, indicating holding and movement against the incoming tide.

evaluating alternative hypothesis of animal movement.

It is also possible to turn the behavior model off completely, or assign more rudimentary circadian behaviors, so that other organisms in the food web relevant to salmonids could be simulated, and salmonid movements can be modeled to forage for food (see Table B.1). The *DSM2,* salinity, water temperature, and turbidity modules can be invoked to produce ecohydraulic simulations so that individuals can be instructed to search for optimal habitat (e.g., Dudley 2019). These latter

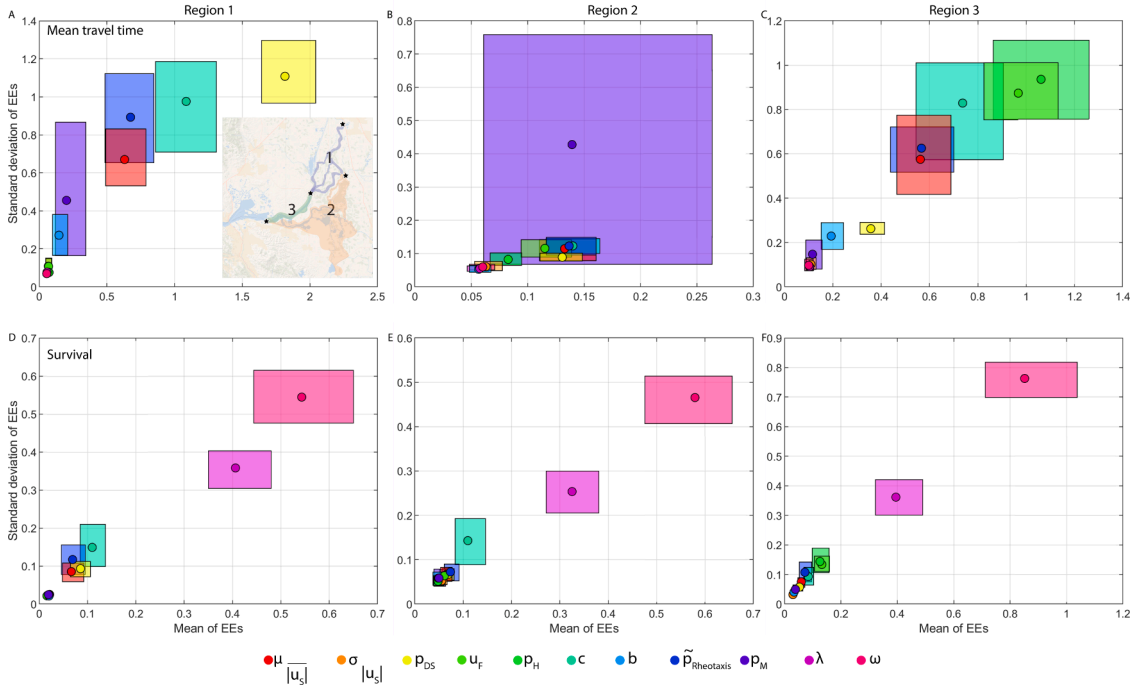

Fig. E.1. Elementary Effects (EE) analysis for the three *toy PTM* regions. A.-C. EEs with respect to the mean travel time. D.-F. EEs with respect to the survival rates. For the pointwise gradient of the model results, each circle and box around it respectively indicates its mean of the absolute value with respect to a parameter on the X-axis and its standard deviation with respect to that parameter on the Y-axis marginalized over all the other parameter values, and bootstrapped confidence bounds. EEs close to zero on both axes indicate that a parameter is unimportant. Large mean and small standard deviation values indicate that a parameter is important by itself. Large standard deviation and small mean values indicate that a parameter is not important by itself, but only becomes important when it interacts with other parameters. Large mean and standard deviation values indicate that a parameter is important both by itself and in interactions with other parameters. Regions correspond to those show in the inset map.

advances would allow us to simulate both rearing and migrating juveniles. In a similar vein, there are no restrictions on the model structure to limit its application to salmonid migration only. The behaviors can be modified to simulate the movements of other species of fish, provided the three key assumptions of one-way coupling between the flow and fish movements, ergodicity of individuals, and non-interacting individuals hold.

Models like the *ePTM* are critical to both planning water operations, and in also bridging the gap between fundamental aquatic biology and water management. As water operations in multipurpose surface water systems are planned over long periods under the influence of climate change and projected water demand and can involve hundreds or even thousands of alternative management scenarios, decision support tools that simulate the effects of flows and water operations on the aquatic ecosystem health over time must be fast. The *ePTM* is easily parallelizable, resulting in linear performance gain with the number of computing cores and high scalability. Under changing landscapes, sea level rise and climate change, models which are not data- and theory-driven will likely be unreliable outside of their calibration range. As we have demonstrated, the *ePTM* can perform reliably even outside its calibration range. Finally, the temporal scale of the behaviors represented in the model are sufficiently fine to resolve biological responses to tidal and daily variability in environmental conditions, but coarse enough so that autocorrelated movements that are difficult to observe in the field can be averaged over. Thus, the *ePTM* is able to represent behaviors which can be supported by the data, and thereby justified to both scientists and managers. The properties of the *ePTM* outlined here constitute the key ingredients in the recipe of a model that can be used to both discover new science about animal movement as well as serve as management tools, viz., (i) high performance, (ii) mechanistic with strong basis in the data and migration theory, and (iii) operating at an intermediate scale of motion.

Data availability statement

The *ePTM* model source code and all the data that was used to calibrate and validate the model are hosted in a GitHub repository at https://github.com/cvclcm/ePTM_v2.

CRediT authorship contribution statement

Vamsi Krishna Sridharan: Conceptualization, Methodology, Software, Validation, Formal analysis, Investigation, Data curation, Visualization, Writing – original draft, Writing – review & editing, Supervision, Project administration, Funding acquisition. **Doug Jackson:** Conceptualization, Methodology, Software, Validation, Formal analysis, Investigation, Writing – original draft, Writing – review & editing. **Andrew M. Hein:** Methodology, Investigation, Formal analysis, Writing – original draft, Writing – review & editing, Funding acquisition. **Russell W. Perry:** Methodology, Formal analysis, Investigation, Data curation, Writing – review & editing. **Adam C. Pope:** Methodology, Formal analysis, Investigation, Data curation, Writing – review & editing. **Noble Hendrix:** Investigation, Writing – review & editing, Project administration, Funding acquisition. **Eric M. Danner:** Resources, Writing – review & editing, Supervision, Project administration, Funding acquisition. **Steven T. Lindley:** Conceptualization, Methodology, Software, Resources, Writing – review & editing, Supervision, Funding acquisition.

Declaration of Competing Interest

The authors declare the following financial interests/personal relationships which may be considered as potential competing interests:

Vamsi Krishna Sridharan reports financial support was provided by California Department of Fish and Wildlife. Vamsi Krishna Sridharan

reports financial support was provided by United States Bureau of Reclamation. Doug Jackson reports financial support was provided by United States Bureau of Reclamation. Andrew Hein reports financial support was provided by National Science Foundation. Andrew Hein reports financial support was provided by California Department of Fish and Wildlife. Eric Danner reports financial support was provided by California Department of Fish and Wildlife. Eric Danner reports financial support was provided by United States Bureau of Reclamation. Steve Lindley reports financial support was provided by California Department of Fish and Wildlife. Steve Lindley reports financial support was provided by United States Bureau of Reclamation. Russel Perry reports financial support was provided by United States Bureau of Reclamation. Adam Pope reports financial support was provided by United States Bureau of Reclamation. Noble Hendrix reports financial support was provided by United States Bureau of Reclamation.

Data availability

Simulating the Migration Dynamics of Juvenile Salmonids Through Rivers and Estuaries Using a Hydrodynamically driven Enhanced Particle Tracking Model (github)

Acknowledgements

Vamsi Krishna Sridharan acknowledges support from the California Department of Fish and Wildlife through Proposition 1 scientific grant P1896007 and from the United States Bureau of Reclamation through cooperative agreement R18AC00096. Doug Jackson acknowledges support from the United States Bureau of Reclamation through cooperative agreement R18AC00096 and interagency agreement R12PG20200. Andrew Hein acknowledges support from California Department of Fish and Wildlife through Proposition 1 scientific grant P1896007 and from the National Science Foundation through grant IOS-1855956. Russell Perry and Adam Pope acknowledge support from the United States Bureau of Reclamation through interagency agreement R19PG00002. Eric Danner and Steven Lindley acknowledge support from the California Department of Fish and Wildlife through Proposition 1 scientific grant P1896007 and the United States Bureau of Reclamation through cooperative agreement R18AC00096 and interagency agreement R12PG20200.

We thank Kate Le and Jacob McQuirk at DWR, Rebecca Buchanan at the University of Washington, Seattle, and Sam Johnston at HTI Sonar for providing the acoustic tracking data used in the model development. Discussions with Pete Klimley at University of California, Davis, Rebecca Buchanan, Patricia Brandes at the United States Fish and Wildlife Service, Jon Burau at the United States Geological Survey (USGS), Rusty Holleman and Edward Gross at Resource Management Associates, Nick Demetras, Peter Dudley, Alyssa Fitzgerald, Cyril Michel and Jeremy Notch and at UCSC, and Dave Rundio and Edward Dick at the National Marine Fisheries Service (NMFS) improved our understanding of fish movements. Similarly, structured engagement supported by the NMFS West Coast Regional Office and USBR helped us leverage the domain expertise of local and regional stakeholders in California. We also thank Drs. Simone Olivetti and Benjamin Burford at the UCSC and Dalton Hance at USGS who supplied additional data used in formulating and validating the model. Lastly, we thank Dr. Simone Olivetti and Ms. Amy Hansen at USGS, the journal editor and two independent reviewers for providing valuable feedback which improved the quality of this manuscript. Any use of trade, firm, or product names is for descriptive purposes only and does not imply endorsement by the U.S. Government.

Appendix A. Structure of the *ePTM*

A.1. Hydrodynamic profiles and tuning parameters

In Section 3.2, we indicated that both straight and curved channels are implemented in the *ePTM*. We determine channel curvature with a statistical estimation procedure in which we fit both a Theil-Sen robust linear regressor (Gilbert 1987), and a Chernov-Lesort robust circular regressor (Chernov, 2010) to a densely up-sampled set of centerline coordinates of the channel. If the Pearson correlation coefficient value of the linear fit exceeds that of the circular fit, or if the estimated radius of curvature exceeds 10Km, the channel is deemed straight. We then determine the angle of the channel bend as the ratio of the total distance along the river and the radius of curvature. Here, only the most significant curvature feature can be represented. A straightforward way to represent smaller-scale meanders is to refine the model grid as needed.

For straight channels, the quantities in the system of Equations (2) are evaluated from the following theoretical profile expressions (DWR, 1998):

$$\begin{aligned} u_H &= U f_V f_H \\ f_L &= A + B\left(\frac{2y}{W}\right)^2 + C\left(\frac{2y}{W}\right)^4 \\ f_V &= \begin{cases} 1 + \left(\frac{0.1}{\kappa}\right)\left[1 + \ln\left(\frac{z}{H}\right)\right]; \frac{z}{H} \geq 0.01 \\ 0; \frac{z}{H} < 0.01 \end{cases} \end{aligned} \tag{A.1}$$

where W and H are respectively the cross-sectional width and depth, U is the mean streamwise water velocity, $\{A, B, C\}$ are constants specific to the river system, $\kappa = 0.41$ is von Karman's constant, f_L and f_V are the lateral and vertical dimensionless water velocity profiles, and

$$\begin{aligned} \varepsilon_H &= C_T H u^* \\ \varepsilon_V &= \kappa \frac{z}{H}\left(1 - \frac{z}{H}\right) \\ \frac{d\varepsilon_V}{dz} &= \kappa \frac{1}{H}\left(1 - 2\frac{z}{H}\right) \\ u^* &\approx 0.1U \end{aligned} \tag{A.2}$$

where $C_T \approx 0.6$ is a constant, and u^* is the friction velocity.

To represent flow profiles in curved channels, we use the results of Gandhi et al. (2016) of turbulent open rectangular channel flow in bends of varying curvature up to 90°. For angles beyond 90°, we assume that the flow adjustment will not be significantly different (Blanckaert and De Vriend, 2004), and so we use the distribution at 90°. We use the best-fit regression of Gandhi et al. (2016) to their results to generate the flow profiles shown in Figure A.1:

$$u(y) = \frac{\log\left[m_1 k_1 \left(\frac{y+1}{2}\right)\right] + \log\left[m_2 k_2 \left(\frac{1-y}{2}\right)\right] + \frac{g_1}{g_2 g_3}\left[\left(\frac{y+1}{2}\right)^{(\alpha-1)}\left(\frac{1-y}{2}\right)^{(\beta-1)}\right]}{\int_0^1 u(\xi)d\xi} \tag{A.3}$$

where m_1, k_1, m_2, k_2, g_1, g_2, g_3, α and β are fitting parameters (Figure A.1A), and ξ is the variable of lateral integration.

Using the force balance between the turbulent eddy diffusivity and the shear stress by assuming a linear decay of the shear stress from its peak value at the channel banks to zero at the lateral position of peak flow defined from the left bank, y_{Max} (and similarly for the right bank),

$$\varepsilon_H \frac{du}{dy} = u^{*2}\left(1 - \frac{y}{y_{\text{Max}}}\right) \tag{A.4}$$

where $\frac{du}{dy}$ is obtained from the data, and smoothing the resulting profile of ε_H to remove spurious discontinuities, we get profiles of the flow and mixing terms.

Per the recommendations in Ross and Sharples (2004), we implemented a mixed layer near the channel banks to eliminate the problem of profile discontinuity. We tested a variety of mixed-layer thicknesses to evaluate the stability constraints in this approach. Based on this analysis, we found that a near-bank and near channel bottom and free surface mixed layer thickness of 20% of the channel width produces only 10% deviation from a uniformly well-mixed concentration profile for passive particles that are initially well mixed laterally.

A.2. Optimal timestep size

To select the optimal value of Δt reported in Section 3.2, we used the absolute value of the deviation of the location of the center of mass from the channel center of an initially uniformly distributed mass of passive particles after two days. We found that a timestep of 20 s produces an optimal tradeoff between runtimes and model consistency.

A.3. Critical streakline estimation

Here, we outline how we estimate the position of the critical streakline introduced in Section 3.7. We compute the position of the critical streakline from the right bank (by convention) as the location till which the flow sums to the outflow nearest to the left bank:

$$\begin{cases} UHW \sum_{\frac{y}{W}=-1}^{\left(\frac{y}{W}\right)_i} u_i = Q_1; \textit{Inflowing channel directed oceanward} \\ UHW \sum_{\frac{y}{W}=-1}^{\left(\frac{y}{W}\right)_i} u_i = Q_2; \textit{Inflowing channel directed landward} \end{cases} \tag{A.5}$$

When an individual reaches a channel junction, it is assigned to one channel or the other based on its lateral location, $y(t)$ (Fig. A.2). When there are junctions with more than three channels, we implement a tree-search algorithm in which the junction is dynamically deconstructed into a sequence of bifurcations with two downstream channels emanating from the channel through which the individual enters the junction.

A.4. XT model formulation in the ePTM

In Section 3.8, we claimed that the parameters of the standard *XT* model as presented in Anderson et al. (2005) are slightly different from those in the *ePTM*. For a fish travelling back and forth a total distance X over n timesteps of size Δt (such that $t = n\Delta t$) through a river reach of length X' with along-stream overground velocities of $u_{i;i=1,2,3,\cdots,n}$, we must have $X' = \bar{u}t$ and $X = |\bar{u}|t$, where $\bar{u} = \frac{\sum_{i=1}^{n} u_i \Delta t}{t}$ and $|\bar{u}| = \frac{\sum_{i=1}^{n} |u_i| \Delta t}{t}$. We can write

$$\begin{aligned} \text{Var}[|u|] &= \text{Var}\left[\sqrt{u^2}\right] \\ &= E\left[u^2\right] - (\text{E}[|u|])^2 \\ &= E\left[u^2\right] - |\bar{u}|^2 \\ \Rightarrow |\bar{u}|^2 &= E[u^2] - \text{Var}[|u|] \\ \Rightarrow |\bar{u}|^2 &= \bar{u}^2 + (\text{Var}[u] - \text{Var}[|u|]) \end{aligned}$$

Clearly, $X \geq X'$, so that we must have $|\bar{u}|^2 \geq \bar{u}^2$, or $\text{Var}[u] - \text{Var}[|u|] \geq 0$.

To account for the dispersion due to random overground movements that includes the effects of biological and hydrodynamic fluctuations over the distance

$$X - X' = \sqrt{(\mathrm{Var}[u] - \mathrm{Var}[|u|])}t$$

in our *XT* model formulation, in addition to the random predator-prey encounters speed defined in Anderson et al. (2005), we must also have an additional term equal to $(\mathrm{Var}[u] - \mathrm{Var}[|u|])t^2$. So, the value of ω in our formulation will be inflated as

$$\omega = \sqrt{\omega'^2 + (\mathrm{Var}[u] - \mathrm{Var}[|u|])} \tag{A.6}$$

over the Anderson et al. (2005) value of ω'.

Now, with survival defined as in Eq. (8), we can establish the equivalence between our and the Anderson et al. formulations by taking the logarithm of the probability of survival as

$$\frac{\sqrt{X'^2 + \omega'^2 t^2}}{\lambda'} = \frac{\sqrt{X^2 + \omega^2 t^2}}{\lambda} \tag{A.7}$$

where λ' is the mean free path-length between predator encounters. For Equation (A.7) to hold, since $\sqrt{X^2 + \omega^2 t^2} \geq \sqrt{X'^2 + \omega'^2 t^2}$, we must have $\lambda \geq \lambda'$, and

$$\lambda = \frac{\sqrt{X^2 + \omega^2 t^2}}{\sqrt{X'^2 + \omega'^2 t^2}}\lambda' \Rightarrow \lambda = \sqrt{\frac{(\bar{u}^2 + \omega'^2) + 2(\mathrm{Var}[u] - \mathrm{Var}[|u|])}{(\bar{u}^2 + \omega'^2)}}\lambda' \tag{A.8}$$

Thus, in our formulation, the ω parameter is inflated by variance due to stochasticity of overground motions in addition to the random encounter speeds of predator-prey interactions, and consequently, the λ parameter is inflated to recover the actual survival rates.

Appendix B. Description of *ePTM* behavior modules

In Section 3, we described the active swimming, orientation, holding and mortality modules in the *ePTM*. We also showed the outcomes for each module as a function of the instantaneous water velocity by holding all the parameters at their calibrated values and looking at the response of the specific module in Fig. 3. Here, we describe the construction of Fig. 3. For these calculations, we first obtained the lengths, X', of each region from Google Earth as the shortest along-river distance from the upstream end to the downstream end of the region.

For the period of 1990 to 2016, we collected water velocities estimated within each *DSM2* channel in each Delta region (Fig. 2) and constructed histograms of water velocities (Fig. 3A). We then classified the regions into three macro-regions: (i) nonreversing macro-region comprising of regions 1 and 2, weakly reversing macro-region comprising of regions 3 to 6, and strongly reversing macro-region comprising of regions 7, 8 and 9 based on the ratio of subtidal low-pass filtered water velocities to root mean squared variability in water velocities. In all subsequent parts of Fig. 3, we used the optimal parameter values in each macro-region to compute the response over a period of five days (or 480 15-minute timesteps) of each behavior module for a single simulated fish to the water velocity bins in each macro-region. We did this by averaging the response in each region within a macro-region weighted by the total along-stream length of the regions. We then smoothed the behavior responses as a function of water velocity using a 6-hour (or 25-point) Savitsky-Golay filter to highlight the signals in Fig. 3.

In Fig. 3B, we used the optimal values of $|\bar{u}_S|$ and $\sigma_{|u_S|}$ to estimate the probability density function of log-normally distributed swimming speeds according to Eq. (3). For each macro-region, we developed a lognormal mixture distribution

$$\mathrm{lnN}(\mu, \sigma) = \sum_{i=1}^{n} \chi_i \mathrm{lnN}(\mu_i, \sigma_i) \tag{B.1}$$

where $\chi_i = \frac{X_i'}{\sum_{i=1}^{n} X_i'}$ is the relative length of region *i*. For each water velocity bin (bin centers of the water velocity histogram), we then drew 480 swimming speeds from the weighted distributions in each macro-region and performed Bernoulli draws to determine fish orientation and holding relative to flow for each of these draws from the estimates in Figs. 3C and 3D below.

In Fig. 3C, we estimated what the likelihood of orienting with the flow. We set an initial orientation with flow, and then ran a MATLAB simulation over 480 timesteps in which at each timestep, first a Bernoulli trial using the optimal value of p_M for the region determined if the orientation persists. If the orientation needed to be changed, then we used the optimal values of $\widetilde{P}_{\mathrm{Rheotaxis}}$, c and b (Section 3.5) with the specified water velocity to find the probability of orienting with the flow. We then performed a second Bernoulli trial using this probability to decide if the orientation remains the same or changes. At each timestep, we kept track of the orientation. We then repeated these steps with an initial orientation against the flow. We then obtained the overall probability of orienting with the flow over a five-day period as the ratio of the total number of timesteps that the simulated fish was oriented with the flow from both starting conditions, and 960.

In Fig. 3D, we estimated what the likelihood of holding is as follows. We started a MATLAB simulation with one individual from day one at 00:00 h to day four at 23:45 h, in which daylight hours were set from 07:00 h to 19:00 h. At each timestep, an individual would hold position if the water velocity was lower than the optimal u_F for the region and if a Bernoulli trial with the optimal value of p_H was successful, or if the timestep fell during the day and a Bernoulli trial with the optimal value of p_{DS} was unsuccessful. We then obtained the overall probability of holding over a five-day period as the ratio of the total number of timesteps that the simulated fish was holding, and 480.

In Fig. 3E, we estimated what the survival probability is for a passive drifter near the water surface. In the nonreversing macro-region, the distance traveled by the individual, $X \approx X'$, and the travel time in the to traverse this distance is nominally

$$t = \frac{X'}{u_H} \tag{B.2}$$

Then, we apply Eq. (8) to estimate the survival. In the reversing macro-regions, we estimated the travel time required to traverse one tidal

excursion, E_X, as

$$t_X = \frac{E_X}{u_H} \tag{B.3}$$

However, over one tidal excursion, the actual displacement of the individual after substitution of Equation (B.3) for t_X is only

$$X_{t_X} = u_S t_X = \frac{u_S}{u_H} E_X \tag{B.4}$$

where $u_S \approx \frac{1.1429}{\sqrt{2}} \frac{\eta_0}{H} u'$ is the Stokes' drift velocity near the water surface for shallow water tidal waves (Sridharan 2018b), $g = 9.81\mathrm{m/s^2}$ is the acceleration due to gravity, η_0 is the amplitude of the tide, H is the average depth of the water column, and u' is the high-frequency tidal fluctuations about the subtidal water velocity. η_0, H and u' were obtained from *DSM2* as respectively, twice the standard deviation of water depths, the average water depth and twice the standard deviation of water velocities in all the channels comprising of the region. Then, the total travel time after substitution of Equations (B.3) and (B.4) respectively, for t_X and X_{t_X} is

$$t = t_X \frac{X'}{X_{t_X}} = 1.24 \frac{H}{\eta_0} \frac{X'}{u_S} \tag{B.5}$$

and the total distance traveled by the individual, after substitution of Equations (B.3) and (B.5) respectively, for t_X and t is

$$X = \frac{t}{t_X} E_X = 1.24 \frac{H}{\eta_0} \frac{u_H}{u_S} X' \tag{B.6}$$

Then, we apply Eq. (8) to estimate the survival. Two interesting feature of Equations (B.2) and (B.6) are that in the nonreversing macro-region, as $\lim_{u_H \to 0} t \to \infty$, so that survival dips, whereas in the reversing macro-regions, as $\lim_{u_H \to 0} X \to \min(X)$, so that survival peaks.

In Table B.1, we show conceptually how relaxing various hypothesized model structures will lead to simpler model formulations and behavior implications. This demonstrates how flexible the *ePTM* is in capturing a wide suite of fish behaviors.

Appendix C. Rationale for constrains on model parameters

Here, we discuss the choice of constraints set on the *ePTM* parameters outlined in Section 4.3.

We surveyed the literature on sustained swimming speeds of Chinook smolts (Dougan 1993; Anglea et al., 2004; Brown et al., 2006; Walker et al., 2016; Lehman et al., 2017) to set the constraints on $|u_S|$ and $\sigma_{|u_S|}$. All of these studies report a maximum sustained swimming speed of about 5 body lengths per second (blps). Based on these studies, we assumed an average fork length of approximately 100 mm, which produces a maximum value of this parameter of 0.5 m/s (Table 1). Setting the maximum $\sigma_{|u_S|}$ also to 0.5 m/s (Table 1) results in more than 95% of the draws rarely exceeding a speed of 10blps for a 100 mm smolt, which is the maximum instantaneous swimming speed observed in the high-resolution fish tracks in the Delta (Lehmann et al. 2017).

Assigning constraints on the orientation parameters was more subjective. For c and b, there are no analogues in the literature. We set these ranges to allow the logistic curve to take on a variety of shapes from linear growth to exponentially saturating within 95% of the range of *DSM2*-modeled water velocities within the Delta between 1962 and 2017.

While there is some background in the literature on diel holding patterns, this is not directly translatable into the holding parameters in the model. For California Central Valley Chinook, Chapman et al. (2013) reported that the proportion of fish detected during the daytime versus the nighttime varied as a function of where they were in the system from 10% to 75%. So, we set the bounds on p_{DS} to encompass these fractions. The tidally-driven holding parameters are more difficult to constrain based on the literature. We therefore computed the peak tidal water velocity modeled in the Delta between 1962 and 2017 using *DSM2* to be 1.5m/s and set this value as the upper limit for u_F. The lower limit for u_F was set at 0 m/s, which would indicate a propensity for individuals to hold even during slack water (Table 1). It is reasonable to expect that not every individual would hold at all times during opposing flow, but p_H could not be directly estimated. We therefore allowed it to vary between 0 and 1 (Table 1).

The bounds on the survival parameters were estimated using a set of *toy PTM* simulations over three regions representing the Delta in a coarse manner (Section C.1). In the simulations, these parameters were allowed to vary over a range of values that produced aggregated survival estimates spanning the range of values reported in the MMR estimates in Perry et al. (2018). The range of these values was then used to bracket the survival parameters in the *ePTM* calibration.

C.1. Toy PTM for initial analysis and screening

In Section 4.3, we referenced a simplified random walk model, the *toy PTM*. This was implemented in the R programming language to screen model parameter interactions and determine the parameter value bounds for optimizing some model parameters. This was implemented as a three-region, one-junction, highly simplified representation of the Delta (Fig. C.1). The *toy PTM* simulates fish movement, routing, and survival through the three regions. An additional region was included within each route solely for the purposes of providing two detection stations within each route, which was required for separately estimating survival in regions 2 and 3 from acoustic telemetry detection data. For this last region, survival is set to one. The movement of individuals from region 1 into regions 2 or 3 is by random chance based on routing probabilities, Ψ for region 2 and $1 - \Psi$ for region 3 (which are equal to the ratios of flows through the regions and the flow in region 1). The *XT* model formulation of Anderson et al. (2005) was adopted to model survival through the regions. The behavior model in the *toy PTM* is identical to that in the *ePTM*. All behavioral and mortality parameters are region-specific.

The *toy PTM* uses water velocities from the Sacramento River from October 2018 to March 2019 to drive the random walk of simulated fish. Region 1 uses water velocities from the Sacramento River at Freeport, Region 2 uses velocities from Sacramento River below the Delta Cross Channel, and Region 3 uses velocities from the Sacramento River at Rio Vista (Fig. 2). We performed multiple runs of the *toy PTM* with 500 simulated fish each time.

Appendix D. Details of the calibration and validation

As we outlined in Section 4.4, we applied a 4-stage calibration process. First, we deduced that the movement (swimming, orientation and holding) parameters could be fit independently of the survival parameters (see below) using the Morris method elementary effects analysis.

Second, to identify the movement parameter set that produced predictions that best aligned with data, we used several methods for evaluating model goodness-of-fit in a 2-level multiobjective optimization refinement. The 2-level refinement was necessary because the goodness-of-fit surfaces contain many local optima. We used three goodness-of-fit measures based on three perspectives in the multiobjective optimization framework. These were the earthmover's distance (an information theoretic measure) between observed and modeled travel times (Levina and Bickel 2001), the log likelihood (a maximum likelihood measure) of observed travel times conditional on *ePTM* parameters (Section D.1), and the intersection over union of the observed and predicted travel time distributions, or the Jaccard index (a visual comparison) (Chung et al., 2019). For each region in the dataset, we defined the overall goodness-of-fit by the sum of the goodness-of-fit measure over all release groups observed in that region. While this results in an exact mathematic value for the log-likelihood, it is only approximately correct in the case of the earthmover's distance and the Jaccard Index. To calculate the earthmover's distance, we used the MATLAB toolbox developed by Yilmaz (2021). We first selected 5000 design points (parameter value sets) using the maximum separation space-filling approach to perform a grid search over. In the three-dimensional space of the three goodness-of-fit measures, we identified the top 10 design points along the Pareto front of performance and selected the top ten of these design points. This Pareto front is the set of design points with the lowest negative log-likelihood, the maximum Jaccard index and the minimum earthmover's distance summed over all releases.

After identifying these candidate optima, we then performed a third step in which we selected 500 new design points each in the vicinity of each candidate optimum using the maximum separation space-filling approach as before to obtain a revised candidate set of 5000 design points. We then repeated the multiobjective analysis as before to identify the top 10% of design points along the new Pareto front within the neighborhoods of the optima from the first iteration. The top performing set of parameter values as defined by the earthmover's index was then chosen as the global optimum for each region. We chose to use the earthmover's distance for selecting the global optima because of its robustness to a small number of fish (<100) within most MMR regions.

Fourth, to fit λ and ω, we used optimal values of all the other parameters, and selected 625 design points, each defined by a pair of values for λ and ω. The goodness-of-fit measure was defined as the sum of the absolute differences between modeled and MMR-predicted survivals for all the releases within a region. The goodness-of-fit surface for the λ and ω parameters is well behaved and has a well-resolved peak, so that a single stage optimization sufficed.

D.1. Log-likelihood goodness-of-fit measure for travel time distributions

In Section 4.4, we outlined the model calibration process, in which one of the goodness-of-fit measures was a log-likelihood of travel time distributions. Here, we show how this is estimated. There are X releases in Y regions, with N_{ij} fish released in the i^{th} release in the j^{th} region. Of the released fish, the number that arrive at the downstream end of the region are $N_{ij}^{'}$. These arrive at ordered times $\mathcal{T}_{ij} = \{t_{ij,1}, t_{ij,2}, \cdots, t_{ij,k}, \cdots, t_{ij,N_{ij}^{'}}\}$. For release i and region j, and for a given design *ePTM* parameter set, there are M replicates for each of the N_{ij} fish. For the k^{th} fish, let there be $M_k^{'}$ replicate simulated arrivals at ordered times $\tau_{ijk,1}, \tau_{ijk,2}, \cdots, \tau_{ijk,M_k^{'}}$. From this set of ordered times, we produce an arrival time distribution $f_{ijks}(t)$ for the k^{th} fish over all the M replicate fish.

Then, the probability of the travel time of the k^{th} individual being $t_{ij,k}$ is

$$P\left(t_{ij,k}\middle|\theta_s\right) = f_{ijks}\left(\tau = t_{ij,k}\middle|\theta_s\right)\cdot d\tau$$

Then, the likelihood of the observed travel time distribution for region i and release j is

$$L_{ij}\left(t_{ij,1}, t_{ij,2}, \cdots, t_{ij,N_{ij}^{'}}\middle|\theta_s\right) = \prod_{k=1}^{N_{ij}^{'}} P\left(t_{ij,k}\middle|\theta_s\right) = d\tau^{N_{ij}^{'}} \prod_{k=1}^{N_{ij}^{'}} f_{ijks}\left(\tau = t_{ij,k}\middle|\theta_s\right)$$

so that the log-likelihood is

$$\log L_{ij}\left(t_{ij,1}, t_{ij,2}, \cdots, t_{ij,N_{ij}^{'}}\middle|\theta_s\right) = N_{ij}^{'}\log d\tau + \sum_{k=1}^{N_{ij}^{'}} \log f_{ijks}\left(\tau = t_{ij,k}\middle|\theta_s\right) \tag{D.1}$$

Now, the log-likelihood across all releases within a given region for θ_s is

$$\log L_j\left(\bigcup_{i=1,j}^{X} \mathcal{T}_{ij}\middle|\theta_s\right) = \left(\sum_{i=1}^{X} N_{ij}^{'}\right)\log d\tau + \sum_{i=1}^{X}\sum_{k=1}^{N_{ij}^{'}} \log f_{ijks}\left(\tau = t_{ij,k}\middle|\theta_s\right) \tag{D.2}$$

Let the set $\theta_j^{\text{Optimal}}$ be the set of values of θ_s that maximizes $\log L_j(\bigcup_{i=1,j}^{X} \mathcal{T}_{ij}\middle|\theta_s)$.

Now, the overall log-likelihood of the data is to be maximized given different parameter combinations in the various regions and releases is

$$\log L\left(\bigcup_{i=1,j=1}^{X,Y} \mathcal{T}_{ij}\middle|\theta_j\right) = \sum_{j=1}^{Y} \log L_j\left(\bigcup_{i=1,j}^{X} \mathcal{T}_{ij}\middle|\theta_j\right) \tag{D.3}$$

Clearly, the $\theta_j^{\text{Optimal}}$s will also maximize the overall log-likelihood of the data.

D.2. Evaluation of space-filling algorithms for initial parameter selection

To select the optimal space-filling algorithm in Section 4.4, we compared 11 algorithms using the R package DiceEval (Dupuy et al., 2015): random selection, naïve and maximin Latin hypercube sampling, Halton, Sobol, Sobol-Owen, Sobol-Faure-Tesuka, and Sobol-Owen-Faure-Tezuka filters, maximum separation criterion, and WSP and Strauss methods. We performed an initial screening with 20 2D points and compared two measures of volume occupancy: (i) the Greenwood statistic, which measures how clumped points are when projected onto a line slicing the 2D plane at various angles, and (ii) the distribution of points along the direction in which the points are most clumped together. Based on this initial assessment, we selected the random selection, maximin Latin hypercube sampling, maximum separation criterion, WSP and Strauss methods as promising candidates for a full evaluation with the 5000 design points.

We subsequently used four measures of volume occupancy: (i) the mesh ratio, which measures the closeness of the designated points to a uniform n-dimensional mesh, (ii) the minimum multidimensional Euclidean separation between points which goes from 0 to 1, (iii) the coverage which measures the deviation of minimum multidimensional separation between points to the mean separation between points, and (iv) the clumpiness of points in all possible two-dimensional projections of the multidimensional points. Using the maximum separation method with a minimum separation criterion of 0.244 produced the best overall performance (Fig. D.1).

D.3. Calibration results

We present the detailed calibration parameter values alluded to in Section 5.1 here in Figs. D.2, D.3 and D.4. Estimates of model parameters are shown for each Delta region in Fig. D.2. In Fig. D.3, we show how the optimal parameter values for each process within the *ePTM* evolve through a simplified schematic network representation of the Delta. The combinations of these parameter values in the *ePTM*'s behavioral modules results in migration patterns that are consistent with the data collected in the Delta (Fig. D.4). We motivate the subsequent discussion using the spatial patterns in Fig. D.3 and the information in Fig. D.4 for various Delta salmonids. In Figure D.4A, we show the distribution of observed swimming speeds. In Figure D.4B, we show that observed fish movements relative to the flow in the high-resolution tracking data are autocorrelated for long periods of time. In Figure D.4C, we show how the migration rate changes as a function of flow. In Figure D.4D, we show how the dispersal of fish changes as a function of flow. In Figure D.4E, we show how fish arrivals vary as a function of the tide phase.

Our analysis of the high-resolution fish tracks in the Delta indicated that there is a large distribution typically between 0 and 10blps in swimming speeds of fish relative to the flow (Figure D.4A). Moreover, we also found that juvenile salmonid movements are temporally autocorrelated for a few minutes on average, with several fish exhibiting long term autocorrelation patterns as well (Figure D.4B). The patterns of large-scale migration rate relative to the mean flow indicate a shift from migration rates that are slower than mean flow, to rates that exceed mean flow as fish move from nonreversing to more tidally reversing conditions (Figure D.4C). We also observed that the dispersal of fish increases as the animals move closer to the ocean (Figure D.4D). These findings indicate a shift in behavior of salmonids with spatial proximity to the ocean. In the tidally reversing macro-regions, there is strong evidence that both steelhead and Chinook salmon move oceanward preferentially during the ebb tide (Figure D.4E).

D.4. Delta-wide XT model

In Section 5.2, to evaluate the flow-survival relationship predicted by *ePTM*, we developed a "Delta-wide" *XT* model as follows. We rewrote the X in Eq. (8) as $\bar{u}t$ and simplified the resulting expression to $P(\text{Survival}) = e^{-\frac{t\sqrt{\bar{u}^2+\omega^2}}{\lambda}}$. Here, $\bar{u}$ is the mean overground movement rate between Delta entry and Chipps Island, $\bar{\lambda}$ is the Delta-wide lengthscale of survival decay, and $X = 99.2$ Km is the distance between Sacramento and Chipps Island along the Sacramento River. Multiplying and dividing the term within the exponentiation by $\bar{u}$ and taking the denominator within the square root, we get $P(\text{Survival}) = e^{-\frac{X}{\lambda}}\sqrt{1+\frac{\omega^2}{\bar{u}^2}}$. A reasonable expectation over the entire scale of the migration distance is that $\bar{u}$ should be proportional to the river flow, Q, and should be a monotonically increasing function of Q. If we assume the simplest possible relationship, i.e., $\bar{u} = \frac{Q}{\bar{A}}$, for some Delta-wide average cross-sectional area $\bar{A}$, then, after simplifying, we get

$$P(\text{Survival}) = e^{-\frac{X}{\lambda}}\sqrt{1+\frac{(\bar{A}\omega)^2}{Q^2}} \tag{D.4}$$

We fit this model by treating $\bar{\lambda}$ and $\bar{A}\omega$ as tuning parameters.

Appendix E. Global sensitivity analysis for the *ePTM*

In Sections 4.4 and 5.4, we applied two GSA approaches outlined below.

E.1. Morris Method

The Morris method starts at a random set of model parameters and cycles through parameter sets by perturbing the value of each parameter a preset number of times while holding the values of the other parameters fixed, until all the parameter values have been perturbed. This process is repeated for a number of trajectories. So, for 33 parameters in the three-region *toy PTM*, we began at 100 randomly chosen parameter value sets within specified bounds (Section 4.4) and ran the *toy PTM* $100 \times (33+1) = 3,400$ times. In each run, ten simulated fish were release every two hours over 13 days for a total of 1560 individuals and the simulations were carried out for three months.

To screen the parameters contributing to the travel time distributions and survival, we used the mean travel time and survival predicted in each region by the *toy PTM* respectively. The Morris method allows us to simultaneously evaluate the importance of each parameter and its interaction with every other parameter as follows. If the mean of the gradient in the model results with respect to a parameter (called the elementary effect) over all the trajectories is small, then this parameter is unimportant on its own. If it is large, then it is important on its own. If the standard deviation in the elementary effect over all the trajectories is small, i.e., the gradient with respect to this parameter does not change by much when the other parameters

change, then this parameter does not interact with other parameters. A large standard deviation likely means that this parameter interacts with other parameters. By performing this analysis with the *toy PTM*, we discovered that travel times are insensitive to the survival parameters and survival is largely sensitive only to the mortality parameters (Fig. E.1).

E.2. Sobol indices

We introduced Sobol indices in the context of ANOVA in Section 5.4. Sobol indices are the first and total order effects estimated using $K\cdot(n+2)$ model calls (for an n-parameter model) at sequentially perturbed parameter values (Baudin et al., 2016). The sequential perturbation of model parameters differentiates this approach from true Monte Carlo sampling. K depends on n, but is typically chosen to be 1,000. These model calls result in three matrices of model results at the set of perturbed values for the i^{th} parameter: (i) two matrices, A and B, containing model results corresponding to independent perturbations of the parameters, and (ii) a matrix $A_B^{(i)}$, in which the i^{th} column of A is replaced by the i^{th} column of B. Then, the first order effect of the i^{th} parameter can be computed by summing the variance in B and $A_B^{(i)}$, which results in (Saltelli et al., 2010)

$$S_i = \underbrace{\frac{1}{K}\sum_{j=1}^{K}\left[f(B_j)\cdot f(B_j)\right]_i}_{\text{Variance due to } i^{\text{th}} \text{ parameter}} + \underbrace{\frac{1}{K}\sum_{j=1}^{K}\left[f(B_j)\cdot f\left(A_B^{(i)}\right)\right]_{\sim i}}_{\substack{\text{Square of}\\ \text{quasi Monte Carlo model mean}}} - \underbrace{f_0^2}_{\substack{\text{Square of}\\ \text{model mean}}} \tag{E.1}$$

The last two terms cancel as $\lim_{K\to\infty}$. The total order effect can be computed by summing the variance in results of the matrices, A and $A_B^{(i)}$, which results in (Saltelli et al., 2010)

$$S_{Ti} = \underbrace{\frac{1}{K}\sum_{j=1}^{K}\left[f(A_j)\cdot f(B_j)\right]_i}_{\substack{\text{Square of}\\ \text{quasi Monte Carlo model mean}}} + \underbrace{\frac{1}{K}\sum_{j=1}^{K}\left[f(A_j)\cdot f\left(A_B^{(i)}\right)\right]_{\sim i}}_{\substack{\text{Variance due to } i^{\text{th}} \text{ parameter}\\ \text{interacting with other parameters}}} - \underbrace{f_0^2}_{\substack{\text{Square of}\\ \text{model mean}}} \tag{E.2}$$

Again, the last two terms cancel. There are many approaches to estimating the first order and total order Sobol indices. Here, we used the Martinez estimator which uses the sum of correlation coefficients between the sets B and A_B, and between the sets A and A_B subtracted from 1 respectively, to estimate the first order and total order Sobol indices for each of the parameters. This is a stable and robust estimator of the Sobol indices which does not suffer from ill-conditioning in many competing approaches (Baudin et al., 2016).

References

AECOM, ICF International, and Turnpenny Horsefield Associates. 2015. *An evaluation of juvenile salmonid routing and barrier effectiveness, predation, and predatory fishes at the head of old river*. Final Report Prepared by the California Department of Water Resources. 494 p. Sacramento, CA. Available at: https://www.researchgate.net/publication/360797376.

Anderson, J.J., Gurarie, E., Zabel, R.W., 2005. Mean free-path length theory of predator–prey interactions: application to juvenile salmon migration. Ecol. Modell. 186 (2), 196–211. https://doi.org/10.1016/j.ecolmodel.2005.01.014.

Anglea, S.M., Geist, D.R., Brown, R.S., Deters, K.A., McDonald, R.D., 2004. Effects of acoustic transmitters on swimming performance and predator avoidance of juvenile Chinook salmon. North Am. J. Fisheries Manag. 24 (1), 162–170. https://doi.org/10.1577/M03-065.

Arenas, A., Politano, M., Weber, L., Timko, M., 2015. Analysis of movements and behavior of smolts swimming in hydropower reservoirs. Ecol. Modell. 312, 292–307. https://doi.org/10.1016/j.ecolmodel.2015.05.015.

Azevedo, R.L. and Parkhurst, Z.E. 1957. *The upper sacramento river salmon and steelhead maintenance program, 1949 - 1956*. United States Fish and Wildlife Service Report.

Baudin, M.E., Bounhaout, K., Delage, T., Iooss, B., Martinez, J.-M., 2016. Numerical stability of Sobol' indices estimateion formula. In: Proceedings of the 8th International Conference on Sensitivity Analysis of Model Output, pp. 50–51. Accessed December 22, 2021. Available at. https://samo2016.sciencesconf.org/data/pages/Proceedings_Samo_2016.pdf.

Berdahl, A., Westley, P.A., Levin, S.A., Couzin, I.D., Quinn, T.P., 2016. A collective navigation hypothesis for homeward migration in anadromous salmonids. Fish and Fisheries 17 (2), 525–542. https://doi.org/10.1111/faf.12084.

Blanckaert, K., De Vriend, H.J., 2004. Secondary flow in sharp open-channel bends. J. Fluid Mech. 498, 353–380. https://doi.org/10.1017/S0022112003006979.

Borthwick, S.M., Corwin, R.R., 2001. *Fish entrainment by archimedes lifts and an internal helical pump at red bluff research pumping plant, upper sacramento river, California: february 1997 - May 2000*. 79p. In: Red Bluff Research Pumping Plant Report Series, 13. United States Bureau of Reclamation, Red Bluff, CA.

Bracis, C., Anderson, J.J, 2012. An investigation of the geomagnetic imprinting hypothesis for salmon. Fish Oceanogr. 21 (2–3), 170–181. https://doi.org/10.1111/j.1365-2419.2012.00617.x.

Brett, J.R., 1971. Energetic responses of salmon to temperature. A study of some thermal relations in the physiology and freshwater ecology of sockeye salmon (Oncorhynchus nerkd). Am. Zool. 11 (1), 99–113. https://doi.org/10.1093/icb/11.1.99.

Brown, R.S., Geist, D.R., Deters, K.A., Grassell, A., 2006. Effects of surgically implanted acoustic transmitters>2% of body mass on the swimming performance, survival and growth of juvenile sockeye and Chinook salmon. J. Fish Biol. 69 (6), 1626–1638. https://doi.org/10.1111/j.1095-8649.2006.01227.x.

Buchanan, R.A., Skalski, J.R., 2020. Relating survival of fall-run Chinook Salmon through the San Joaquin Delta to river flow. Environ. Biol. Fishes 103 (5), 389–410. https://doi.org/10.1007/s10641-019-00918-y.

Burke, B.J., Anderson, J.J., Baptista, A.M., 2014. Evidence for multiple navigational sensory capabilities of Chinook salmon. Aquat. Biol. 20 (1), 77–90. https://doi.org/10.3354/ab00541.

California Department of Water Resources, 1998. Methodology for flow and salinity estimates in the Sacramento-San Joaquin Delta and Suisun Marsh. In: Nineteenth Annual Progress Report to the State Water Resources Control Board. Sacramento, CA, p. 170. Accessed December 24, 2021. Available at: https://data.cnra.ca.gov/dataset/methodology-for-flow-and-salinity-estimates-in-the-sacramento-san-joaquin-delta-and-suisun-marsh/resource/44093c61-51fe-411f-8425-efc167d1ec6f.

California Department of Water Resources, 2015. Final Project Report. Bay-Delta Office, Sacramento, California, p. 298.

California Department of Water Resources, 2016. Final Project Report. Bay-Delta Office, Sacramento, California, p. 486.

Chapman, E.D., Hearn, A.R., Michel, C.J., Ammann, A.J., Lindley, S.T., Thomas, M.J., Singer, G.P., Peterson, M.L., MacFarlane, R.B., Klimley, A.P., 2013. Diel movements of out-migrating Chinook salmon (Oncorhynchus tshawytscha) and steelhead trout (Oncorhynchus mykiss) smolts in the Sacramento/San Joaquin watershed. Environ. Biol. Fishes 96 (2), 273–286. https://doi.org/10.1007/s10641-012-0001-x.

Chernov, N., 2010. Circular and Linear Regression: Fitting Circles and Lines By Least Squares. CRC Press, p. 286.

Chung, N.C., Miasojedow, B., Startek, M., Gambin, A., 2019. Jaccard/Tanimoto similarity test and estimation methods for biological presence-absence data. BMC Bioinf. 20 (15), 1–11. https://doi.org/10.1186/s12859-019-3118-5.

Codling, E.A., Plank, M.J., Benhamou, S., 2008. Random walk models in biology. J. Royal Soc. Interface 5 (25), 813–834. https://doi.org/10.1098/rsif.2008.0014.

Dancik, G.M., Jones, D.E., Dorman, K.S., 2010. Parameter estimation and sensitivity analysis in an agent-based model of Leishmania major infection. J. Theor. Biol. 262 (3), 398–412. https://doi.org/10.1016/j.jtbi.2009.10.007.

Delta Stewardship Council, 2019. Delta Science plan: vision, Principles and Approaches For Integrating and Coordinating Science in the Delta. Delta Science Program, p. 104. Accessed December 24, 2021. Available at. https://deltacouncil.ca.gov/pdf/2019-delta-science-plan.pdf.

Delta Stewardship Council, 2022. 2022-2026 Science Action Agenda. Delta Science Program, Sacramento, California, p. 106. Final DraftAccessed May 9, 2022. Available at. https://scienceactionagenda.deltacouncil.ca.gov/pdf/2022-2026-science-action-agenda.pdf.

Dougan, M.C., 1993. Doctoral Thesis. University of Canterbury, Christchurch, New Zealand.

Dudley, P.N., 2019. Insights from an individual based model of a fish population on a large regulated river. Environ. Biol. Fishes 102 (8), 1069–1095. https://doi.org/10.1007/s10641-019-00891-6.

Dupuy, D., Helbert, C., Franco, J., 2015. DiceDesign and DiceEval: two R packages for design and analysis of computer experiments. J. Stat. Softw. 65 (11) https://doi.org/10.18637/jss.v065.i11.

Filella, A., Nadal, F., Sire, C., Kanso, E., Eloy, C, 2018. Model of collective fish behavior with hydrodynamic interactions. Phys. Rev. Lett. 120 (19), 198101 https://doi.org/10.1103/PhysRevLett.120.198101.

Floryan, D., Van Buren, T., Smits, A.J., 2018. Efficient cruising for swimming and flying animals is dictated by fluid drag. Proceed. Nat. Acad. Sci. 115 (32), 8116–8118. https://doi.org/10.1073/pnas.1805941115.

Forward Jr., R.B., Tankersley, R.A., 2001. Selective tidal-stream transport of marine animals. Oceanography and Marine Biology, an Annual Review. CRC Press.

Gandhi, B.K., Verma, H.K., Abraham, B, 2016. Mathematical modeling and simulation of flow velocity profile for rectangular open channels. ISH J. Hydraulic Eng. 22 (2), 193–203. https://doi.org/10.1080/09715010.2015.1136244.

Gilbert, R.O., 1987. Sen's Nonparametric Estimator of Slope. Statistical Methods For Environmental Pollution Monitoring. John Wiley and Sons, pp. 217–219. ISBN: 978-0-471-28878-7.

Goodwin, R.A., Lai, Y.G., Taflin, D.E., Smith, D.L., McQuirk, J., Trang, R., and Reeves, R.. In rev. Cognitive architecture predicting fish swim paths in 3-D, 2-D time-varying river hydrodynamics for engineering design of infrastructure.

Goodwin, R.A., Nestler, J.M., Anderson, J.J., Weber, L.J., Loucks, D.P., 2006. Forecasting 3-D fish movement behavior using a Eulerian–Lagrangian–agent method (ELAM). Ecol. Modell. 192 (1–2), 197–223. https://doi.org/10.1016/j.ecolmodel.2005.08.004.

Gross, E., Saenz, B., Rachiele, R., Grinbergs, S., Grimaldo, L., Korman, J., Smith, P., MacWilliams, M. and Bever, A., 2020. *Study 2–distribution estimates for hypothesized swimming behaviors and statistical evaluation of particle-tracking models predicting proportional entrainment loss*. Prepared for Collaborative Science and Adaptive Management Program's Collaborative Adaptive Management Team. 178 p.

Gross, E.S., Holleman, R.C., Thomas, M.J., Fangue, N.A., Rypel, A.L., 2021. Development and evaluation of a Chinook Salmon Smolt swimming behavior model. Water (Basel) 13 (20), 2904. https://doi.org/10.3390/w13202904.

Hance, D.J., Perry, R.W., Burau, J.R., Blake, A., Stumpner, P., Wang, X., Pope, A., 2020. Combining models of the critical streakline and the cross-sectional distribution of juvenile salmon to predict fish routing at river junctions. San Francisco Estuary and Watershed Sci. 18 (1) https://doi.org/10.15447/sfews.2020v18iss1art3.

Healey, M.C., 1980. Utilization of the Nanaimo River estuary by juvenile Chinook salmon, Oncorhynchus tshawytscha. Fishery Bullet. 77 (3).

Hedger, R.D., Martin, F., Hatin, D., Caron, F., Whoriskey, F.G., Dodson, J.J., 2008. Active migration of wild Atlantic salmon Salmo salar smolt through a coastal embayment. Mar. Ecol. Prog. Ser. 355, 235–246. https://doi.org/10.3354/meps07239.

Hein, A.M., Gil, M.A., Twomey, C.R., Couzin, I.D., Levin, S.A., 2018. Conserved behavioral circuits govern high-speed decision-making in wild fish shoals. Proceed. Nat. Acad. Sci. 115 (48), 12224–12228. https://doi.org/10.1073/pnas.1809140115.

Iooss, B. 2021. *Package 'sensitivity.'* CRAN repository. Accessed December 22, 2021. Available at: https://cran.r-project.org/web/packages/sensitivity/sensitivity.pdf.

Iooss, B., Lemaître, P., 2015. A Review On Global Sensitivity Analysis Methods. In Uncertainty Management in Simulation-Optimization of Complex Systems. Springer, Boston, MA, pp. 101–122.

Irarrázaval, F., Bustos-Gallardo, B., 2019. Global salmon networks: unpacking ecological contradictions at the production stage. Econ. Geogr. 95 (2), 159–178. https://doi.org/10.1080/00130095.2018.1506700.

Jhawar, J., Morris, R.G., Amith-Kumar, U.R., Raj, M.D., Rogers, T., Rajendran, H., Guttal, V., 2020. Noise-induced schooling of fish. Nat. Phys. 16 (4), 488–493. https://doi.org/10.1038/s41567-020-0787-y.

Johnson, R.C., Windell, S., Brandes, P.L., Conrad, J.L., Ferguson, J., Goertler, P.A., Harvey, B.N., Heublein, J., Israel, J.A., Kratville, D.W., Kirsch, J.E., 2017. Science advancements key to increasing management value of life stage monitoring networks for endangered Sacramento River Winter-run Chinook salmon in California. San Francisco Estuary and Watershed Sci. 15 (3) https://doi.org/10.15447/sfews.2017v15iss3art1.

Kelly, J.T., Klimley, A.P., 2012. Relating the swimming movements of green sturgeon to the movement of water currents. Environ. Biol. Fishes 93 (2), 151–167. https://doi.org/10.1007/s10641-011-9898-8.

Kimmerer, W.J., 2008. Losses of Sacramento river Chinook salmon and delta smelt to entrainment in water diversions in the Sacramento–San Joaquin Delta. San Francisco Estuary and Watershed Sci. 6 (2) https://doi.org/10.15447/sfews.2008v6iss2art2.

Kimmerer, W.J., Rose, K.A., 2018. Individual-based modeling of delta smelt population dynamics in the Upper San Francisco Estuary III. Effects of entrainment mortality and changes in prey. Trans. Am. Fish. Soc. 147 (1), 223–243. https://doi.org/10.1002/tafs.10015.

Kjelson, M.A., Raquel, P.F., Fisher, F.W., 1982. Life history of fall-run juvenile Chinook salmon, Oncorhynchus tshawytscha, in the Sacramento-San Joaquin estuary, California. Estuarine Comparisons. Academic Press, pp. 393–411. https://doi.org/10.1016/B978-0-12-404070-0.50029-6.

Klimley, A.P., Wyman, M.T., Kavet, R., 2017. Chinook salmon and green sturgeon migrate through San Francisco Estuary despite large distortions in the local magnetic field produced by bridges. PLoS ONE 12 (6), e0169031. https://doi.org/10.1371/journal.pone.0169031.

Lacroix, G.L., McCurdy, P., 1996. Migratory behaviour of post-smolt Atlantic salmon during initial stages of seaward migration. J. Fish Biol. 49 (6), 1086–1101. https://doi.org/10.1111/j.1095-8649.1996.tb01780.x.

Lacroix, G.L., Knox, D., Stokesbury, M.J.W., 2005. Survival and behaviour of post-smolt Atlantic salmon in coastal habitat with extreme tides. J. Fish Biol. 66 (2), 485–498. https://doi.org/10.1111/j.0022-1112.2005.00616.x.

Lai, Y.G., 2022. Flow characteristics at a river diversion juncture and implications for juvenile salmon entrainment. Fluids 7 (3), 98. https://doi.org/10.3390/fluids7030098.

Lehman, B., Huff, D.D., Hayes, S.A., Lindley, S.T., 2017. Relationships between Chinook salmon swimming performance and water quality in the San Joaquin River, California. Trans. Am. Fish. Soc. 146 (2), 349–358. https://doi.org/10.1080/00028487.2016.1271827.

Levina, E., Bickel, P., 2001. The earth mover's distance is the mallows distance: some insights from statistics. In: Proceedings Eighth IEEE International Conference on Computer Vision, 2. IEEE, pp. 251–256. https://doi.org/10.1109/ICCV.2001.937632.

Liao, J.C., 2007. A review of fish swimming mechanics and behaviour in altered flows. Philosophical Trans. Royal Soc. B: Biol. Sci. 362 (1487), 1973–1993. https://doi.org/10.1098/rstb.2007.2082.

Lohmann, K.J., Lohmann, C.M., 2019. There and back again: natal homing by magnetic navigation in sea turtles and salmon. J. Experimental Biol. 222 (Suppl_1), jeb184077 https://doi.org/10.1242/jeb.184077.

MacFarlane, R.B., Norton, E.C., 2002. Physiological ecology of juvenile chinook salmon (Oncorhynchus tshawytscha) at the southern end of their distribution, the San Francisco Estuary and Gulf of the Farallones, California. Fishery Bullet. 100 (2), 244–257.

Mains, E.M., Smith, J.M., 1964. The distribution, size, time, and current preferences of seaward migrant chinook salmon in the Columbia and Snake Rivers. Fish. Res. 2 (3), 5–43.

Martin, B.T., Gil, M.A., Fahimipour, A.K., Hein, A.M., 2021. Informational constraints on predator–prey interactions. Oikos. https://doi.org/10.1111/oik.08143.

Massoudieh, A., Loboschefsky, E., Sommer, T., Ginn, T., Rose, K., Loge, F., 2011. Spatio-temporal modeling of striped-bass egg, larval movement, and fate in the San Francisco Bay–Delta. Ecol. Modell. 222 (19), 3513–3523. https://doi.org/10.1016/j.ecolmodel.2011.08.009.

McCleave, J.D., 1978. Rhythmic aspects of estuarine migration of hatchery-reared Atlantic salmon (Salmo salar) smolts. J. Fish Biol. 12 (6), 559–570. https://doi.org/10.1111/j.1095-8649.1978.tb04202.x.

McCormick, S.D., Hansen, L.P., Quinn, T.P., Saunders, R.L., 1998. Movement, migration, and smolting of Atlantic salmon (Salmo salar). Canadian J. Fisheries and Aquatic Sci. 55 (S1), 77–92. https://doi.org/10.1139/d98-011.

Michel, C.J., Ammann, A.J., Lindley, S.T., Sandstrom, P.T., Chapman, E.D., Thomas, M. J., Singer, G.P., Klimley, A.P., MacFarlane, R.B., 2015. Chinook salmon outmigration survival in wet and dry years in California's Sacramento River. Canadian J. Fisheries and Aquatic Sci. 72 (11), 1749–1759. https://doi.org/10.1139/cjfas-2014-0528.

Michel, C.J., Henderson, M.J., Loomis, C.M., Smith, J.M., Demetras, N.J., Iglesias, I.S., Lehman, B.M., Huff, D.D., 2020. Fish predation on a landscape scale. Ecosphere 11 (6), e03168. https://doi.org/10.1002/ecs2.3168.

Michel, C.J., Notch, J.J., Cordoleani, F., Ammann, A.J., Danner, E.M., 2021. Nonlinear survival of imperiled fish informs managed flows in a highly modified river. Ecosphere 12 (5), e03498. https://doi.org/10.1002/ecs2.3498.

Miles, J., Vowles, A.S., Kemp, P.S., 2021. The response of common minnows, Phoxinus phoxinus, to visual cues under flowing and static water conditions. Anim. Behav. 179, 289–296. https://doi.org/10.1016/j.anbehav.2021.07.004.

Miller, B.A., Sadro, S., 2003. Residence time and seasonal movements of juvenile Coho salmon in the ecotone and lower estuary of Winchester Creek, South Slough, Oregon. Trans. Am. Fish. Soc. 132 (3), 546–559. https://doi.org/10.1577/1548-8659(2003)132<0546:RTASMO>2.0.CO;2.

Moore, A., Ives, S., Mead, T.A., Talks, L., 1998. The migratory behaviour of wild Atlantic salmon (Salmo salar L.) smolts in the River Test and Southampton Water, southern England, 295-204 Advances in Invertebrates and Fish Telemetry. Springer, Dordrecht, The Netherlands.

Morrice, K.J., Baptista, A.M., Burke, B.J., 2020. Environmental and behavioral controls on juvenile Chinook salmon migration pathways in the Columbia River estuary. Ecol. Modell. 427, 109003 https://doi.org/10.1016/j.ecolmodel.2020.109003.

Moser, M.L., Olson, A.F., Quinn, T.P., 1991. Riverine and estuarine migratory behavior of coho salmon (Oncorhynchus kisutch) smolts. Canadian J. Fisheries and Aquatic Sci. 48 (9), 1670–1678. https://doi.org/10.1139/f91-198.

Moyle, P.B., Bennett, W.A., Dahm, C., Durand, J.R., Enright, C., Fleenor, W.E., Kimmerer, W., and Lund, J.R. 2010. *Changing ecosystems: a brief ecological history of the Delta*. Report to the California State Water Resources Control Board, Sacramento, CA. Accessed December 4, 2021. Available at: https://www.researchgate.net/profile/John-Durand/publication/235350728_Changing_ecosystems_a_brief_ecological_history_of_the_Delta/links/0fcfd51132ee97c637000000/Changing-ecosystems-a-brief-ecological-history-of-the-Delta.pdf.

Nadler, L.E., McCormick, M.I., Johansen, J.L., Domenici, P., 2021. Social familiarity improves fast-start escape performance in schooling fish. Commun. Biol. 4 (1), 1–10. https://doi.org/10.1038/s42003-021-02407-4.

Nagel, C., Mueller, M., Pander, J., Stoeckle, B.C., Kuehn, R., Geist, J., 2021. Going with the flow: spatio-temporal drift patterns of larval fish in a large Alpine river. Freshw. Biol. 66 (9), 1765–1781. https://doi.org/10.1111/fwb.13790.

National Marine Fisheries Service. 2021. *Winter-run Chinook salmon lifecycle model: workshops*. Accessed December 24, 2021. Available at: https://oceanview.pfeg.noaa.gov/wrlcm/resources.

Newman, K.B., 2003. Modelling paired release-recovery data in the presence of survival and capture heterogeneity with application to marked juvenile salmon. Stat. Modelling. 3 (3), 157–177. https://doi.org/10.1191/1471082X03st055oa.

Notch, J., Robinson, R., Pham, T., Logston, R., McHuron, A., Ammann, A., Michel, C., 2020. Annual Report Prepared by University of California – Santa Cruz for the U.S. Bureau of Reclamation under contract USDI/BOR# R18AC00039. Accessed December 23, 2021. Available at: https://oceanview.pfeg.noaa.gov/CalFishTrack/.

Notch, J., Robinson, R., Pham, T., Logston, R., McHuron, A., Ammann, A., Michel, C., 2021. Final Report Prepared by University of California – Santa Cruz for the U.S. Bureau of Reclamation under contract USDI/BOR# R18AC00039. Accessed December 23, 2021. Available at: https://oceanview.pfeg.noaa.gov/CalFishTrack/.

Olivetti, S., Gil, M.A., Sridharan, V.K., Hein, A.M., 2021. Merging computational fluid dynamics and machine learning to reveal animal migration strategies. Methods in Ecol. Evolution 12, 1186–1200. https://doi.org/10.1111/2041-210X.13604.

Oteiza, P., Odstrcil, I., Lauder, G., Portugues, R., Engert, F., 2017. A novel mechanism for mechanosensory-based rheotaxis in larval zebrafish. Nature 547 (7664), 445–448. https://doi.org/10.1038/nature23014.

Owen, A.B., 2013. Variance components and generalized Sobol'indices. SIAM/ASA J. *Uncertainty Quantification* 1 (1), 19–41. https://doi.org/10.1137/120876782.

Pauly, D., 2018. A vision for marine fisheries in a global blue economy. Mar. Policy 87, 371–374. https://doi.org/10.1016/j.marpol.2017.11.010.

Perry, R.W., Buchanan, R.A., Brandes, P.L., Burau, J.R., Israel, J.A., 2016. Anadromous salmonids in the Delta: new science 2006–2016. San Francisco Estuary and Watershed Sci. 14 (2) https://doi.org/10.15447/sfews.2016v14iss2art7.

Perry, R.W., Pope, A.C., Romine, J.G., Brandes, P.L., Burau, J.R., Blake, A.R., Ammann, A.J., Michel, C.J., 2018. Flow-mediated effects on travel time, routing, and survival of juvenile Chinook salmon in a spatially complex, tidally forced river delta. Canadian J. Fisheries and Aquatic Sci. 75 (11), 1886–1901. https://doi.org/10.1139/cjfas-2017-0310.

Perry, R.W., Romine, J.G., Adams, N.S., Blake, A.R., Burau, J.R., Johnston, S.V., Liedtke, T.L., 2014. Using a non-physical behavioural barrier to alter migration routing of juvenile chinook salmon in the Sacramento–San Joaquin River delta. River Res. Appl. 30 (2), 192–203. https://doi.org/10.1002/rra.2628.

Perry, R.W., Skalski, J.R., Brandes, P.L., Sandstrom, P.T., Klimley, A.P., Ammann, A., MacFarlane, B., 2010. Estimating survival and migration route probabilities of juvenile Chinook salmon in the Sacramento–San Joaquin River Delta. North Am. J. Fisheries Manag. 30 (1), 142–156. https://doi.org/10.1577/M08-200.1.

Pianosi, F., Wagener, T., 2015. A simple and efficient method for global sensitivity analysis based on cumulative distribution functions. Environ. Modell. Software 67, 1–11. https://doi.org/10.1016/j.envsoft.2015.01.004.

Poli, R., Kennedy, J., Blackwell, T., 2007. Particle swarm optimization. Swarm intelligence 1 (1), 33–57.

W. Pope, A.C., Perry, R., Harvey, B.N., Hance, D.J., Hansel, H.C, 2021. Juvenile Chinook salmon survival, travel time, and floodplain use relative to riverine channels in the Sacramento–San Joaquin River Delta Trans. Am. Fish. Soc. 150, 38–55. https://doi.org/10.1002/tafs.10271.

Raimondi, P., Hein, A., Sridharan, V., Danner, E., and Lindley, S. 2021. *A next-generation model of juvenile salmon migration through the Sacramento-San Joaquin Delta*. Final Report Submitted to the California Department of Fish and Wildlife Under Agreement No. P1896007. 55 p. Santa Cruz, California.

Ramón, C.L., Acosta, M., Rueda, F.J., 2018. Hydrodynamic drivers of juvenile-salmon out-migration in the Sacramento River: secondary circulation. J. Hydraulic Eng. 144 (8), 04018042 https://doi.org/10.1061/(ASCE)HY.1943-7900.0001484.

Ross, O.N., Sharples, J., 2004. Recipe for 1-D Lagrangian particle tracking models in space-varying diffusivity. Limnol. Oceanography: Methods 2 (9), 289–302. https://doi.org/10.4319/lom.2004.2.289.

Rundio, D.E., Montogomery, A.N., Nesbit, M.G., Morris, M.S., Brooks, G.T., Axel, G.A., Lamb, J.J., Zabel, R.W., Ferguson, J., Lindley, S.T., 2017. NOAA Technical Memorandum No. 573, p. 130. https://doi.org/10.7289/V5/TM-SWFSC-573.

Saltelli, A., Annoni, P., Azzini, I., Campolongo, F., Ratto, M., Tarantola, S., 2010. Variance based sensitivity analysis of model output. Design and estimator for the total sensitivity index. Comput. Phys. Commun. 181 (2), 259–270. https://doi.org/10.1016/j.cpc.2009.09.018.

San Joaquin River Group Authority, 2013. On implementation and monitoring of the San Joaquin River agreement and the Vernalis Adaptive Management Plan (VAMP). In: 2011 Annual Technical Report. Accessed December 24, 2021. Available at: https://www.fws.gov/lodi/salmonid_survival_studies/juvenile_salmonid_survival_reports/.

Scranton, K., Knape, J., de Valpine, P., 2014. An approximate Bayesian computation approach to parameter estimation in a stochastic stage-structured population model. Ecology 95 (5), 1418–1428. https://doi.org/10.1890/13-1065.1.

Smith, J.R., 1974. Distribution of seaward migrating chinook salmon and steelhead trout in the Snake River above Lower Monumental Dam. Marine Fisheries Rev. 36 (8), 42–45.

Smythe, B., 2020. All Things Flow – Fluid Mechanics For the Natural Sciences. LibreTexts Project. Accessed May 11, 2022. Available at. https://eng.libretexts.org/Bookshelves/Civil_Engineering/Book%3A_All_Things_Flow_-_Fluid_Mechanics_for_the_Natural_Sciences_(Smyth).

Solomon, D.J., 1978. Some observations on salmon smolt migration in a chalkstream. J. Fish Biol. 12 (6), 571–574. https://doi.org/10.1111/j.1095-8649.1978.tb04203.x.

Sridharan, V.K., Hein, A.M., 2019. Analytical solution of advection-dispersion boundary value processes in environmental flows. Water Resour. Res. 55 (12), 10130–10143. https://doi.org/10.1029/2019WR025429.

Sridharan, V.K., Jackson, D., Perry, R., Pope, A., Hendrix, N., Hein, A.M., Danner, E.M., and Lindley, S.T. 2021. Enhanced Particle tracking model (ePTM) (Version 2.0) [Computer software]. Available at: https://github.com/cvclcm/ePTM_v2.

Sridharan, V.K., Monismith, S.G., Fong, D.A., Hench, J.L., 2018a. One-dimensional particle tracking with streamline preserving junctions for flows in channel networks. J. Hydraulic Eng. 144 (2), 04017063 https://doi.org/10.1061/(ASCE)HY.1943-7900.0001399.

Sridharan, V.K., Monismith, S.G., Fringer, O.B., Fong, D.A., 2018b. Evaluation of the delta simulation model-2 in computing tidally driven flows in the Sacramento-San Joaquin Delta. San Francisco Estuary and Watershed Sci. 16 (2) https://doi.org/10.15447/sfews.2018v16iss2art6.

Steel, A.E., Sandstrom, P.T., Brandes, P.L., Klimley, A.P., 2013. Migration route selection of juvenile Chinook salmon at the delta cross channel, and the role of water velocity and individual movement patterns. Environ. Biol. Fishes 96 (2), 215–224. https://doi.org/10.1007/s10641-012-9992-6.

Steel, A.E., Anderson, J.J., Mulvey, B., Smith, D.L., 2020. Applying the mean free-path length model to juvenile Chinook salmon migrating in the Sacramento River, California. Environ. Biol. Fishes 103, 1603–1617. https://doi.org/10.1007/s10641-020-01046-8.

Sturrock, A.M., Wikert, J.D., Heyne, T., Mesick, C., Hubbard, A.E., Hinkelman, T.M., Johnson, R.C., 2015. Reconstructing the migratory behavior and long-term survivorship of juvenile Chinook salmon under contrasting hydrologic regimes. PLoS ONE 10 (5), e0122380. https://doi.org/10.1371/journal.pone.0122380.

Verhelst, P., Bruneel, S., Reubens, J., Coeck, J., Goethals, P., Oldoni, D., Moens, T., Mouton, A., 2018. Selective tidal stream transport in silver European eel (Anguilla Anguilla L.) – migration behavior in a dynamic estuary. Estuar. Coast Shelf Sci. 213, 260–268. https://doi.org/10.1016/j.ecss.2018.08.025.

Videler, J.J., Nolet, B.A., 1990. Costs of swimming measured at optimum speed: scale effects, differences between swimming styles, taxonomic groups and submerged and surface swimming. *Comparative Biochem. Physiol. A, Comparative Physiol.* 97 (2), 91–99. https://doi.org/10.1016/0300-9629(90)90155-l.

Visser, A.W., 1997. Using random walk models to simulate the vertical distribution of particles in a turbulent water column. Mar. Ecol. Prog. Ser. 158, 275–281. https://doi.org/10.3354/meps158275.

Walker, R.W., Ashton, N.K., Brown, R.S., Liss, S.A., Colotelo, A.H., Beirão, B.V., Townsend, R.L., Deng, Z.D., Eppard, M.B., 2016. Effects of a novel acoustic transmitter on swimming performance and predator avoidance of juvenile Chinook Salmon: determination of a size threshold. Fish. Res. 176, 48–54. https://doi.org/10.1016/j.fishres.2015.12.007.

Yeakley, J.A., Hughes, R.M., 2014. Global and regional context of salmonids and urban areas. Wild Salmonids in the Urbanizing Pacific Northwest. Springer, New York, NY, pp. 11–29. Accessed December 23, 2021. Available at: https://scholar.archive.org/work/hvsimbwx2nclvmgcpb7jhau2hu/access/wayback/http://www.springer.com/cda/content/document/cda_downloaddocument/9781461488170-c1.pdf?SGWID=0-0-45-1428008-p175373186.

Yilmaz, U., 2021. The Earth Mover's Distance. MATLAB Central File Exchange. . Accessed December 24, 2021. Available at: https://www.mathworks.com/matlabcentral/fileexchange/22962-the-earth-mover-s-distance.

Zabel, R.W., Anderson, J.J., 1997. A model of the travel time of migrating juvenile salmon, with an application to Snake River spring chinook salmon. North Am. J. Fisheries Manag. 17 (1), 93–100. https://doi.org/10.1577/1548-8675(1997)017<0093:AMOTTT>2.3.CO;2.

Zabel, R.W., Faulkner, J., Smith, S.G., Anderson, J.J., Van Holmes, C., Beer, N., Iltis, S., Krinke, J., Fredricks, G., Bellerud, B., Sweet, J., Giorgi, A, 2008. Comprehensive passage (COMPASS) model: a model of downstream migration and survival of juvenile salmonids through a hydropower system. Hydrobiologia 609 (1), 289–300. https://doi.org/10.1007/s10750-008-9407-z.